2021-05

A rules-based shoreface translation and sediment budgeting tool for estimating coastal change: ShoreTrans

McCarroll, Jak

10.1016/j.margeo.2021.106466
Marine Geology
Elsevier

Marine Geology 435 (2021) 106466

Contents lists available at ScienceDirect

Marine Geology

journal homepage: www.elsevier.com/locate/margo

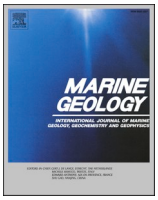

A rules-based shoreface translation and sediment budgeting tool for estimating coastal change: ShoreTrans

R. Jak McCarroll [a,b,*], Gerd Masselink [a], Nieves G. Valiente [c], Timothy Scott [a], Mark Wiggins [a], Josie-Alice Kirby [a], Mark Davidson [a]

[a] School of Biological and Marine Sciences, Plymouth University, Drake Circus, PL4 8AA, Plymouth, UK
[b] Department of Environment, Land, Water and Planning, East Melbourne, Victoria, 3002, Australia
[c] Met Office, Fitzroy Road, EX1 3PB, Exeter, UK

ARTICLE INFO

Keywords:
Sea level rise
Multi-decadal coastal evolution
Shoreline modelling
Bruun rule

ABSTRACT

Predicting change to shorelines globally presents an increasing challenge as sea level rise (SLR) accelerates. Many shoreline prediction models use the simplistic 'Bruun rule' for dealing with SLR profile translation, in-part due to alternative approaches being too complex and time-consuming to implement. To address this, we introduce ShoreTrans: a simple, rules-based, user-input driven, shoreface translation and sediment budgeting model, that applies the surveyed 2D-profile (not a parameterization), for estimating change to realistic coastlines, resulting from SLR and variations in sediment supply, while accounting for armouring, hard-rock cliffs and outcropping rocks. The tool can be applied to sand, gravel, rock and engineered coasts at a temporal scale of 10–100 years, accounting for shoreline trends as well as variability. The method accounts for: (1) dune encroachment/accretion; (2) barrier rollback; (3) non-erodible layers; (4) seawalls; (5) lower shoreface transport; (6) alongshore rotation; and (7) other sources and sinks. Uncertainty is accounted for using a probabilistic distribution for inputs and Monte Carlo simulations. We provide a first-pass assessment of two macrotidal UK embayments: Perranporth (sandy, dissipative, cross-shore dominant transport) and Start Bay (gravel, reflective, bi-directional alongshore dominant), then use idealised profiles to investigate the relative importance of forcing controls on shoreline recession and beach width. For the dissipative sandy site, the primary modes of coastal change are predicted to be short-term storm erosion and SLR translation while long-term trends may be important but are highly uncertain. For the reflective gravel site, the primary mode is multi-decadal longshore sediment flux, while short-term alongshore rotation and SLR translation are secondary. Relative to the ShoreTrans approach, the Bruun rule under-predicts shoreline recession in front of cliffs, seawalls and for low barriers that rollback, and over-predicts where large erodible dunes are present. ShoreTrans directly addresses change in beach width, with beaches in front of seawalls and cliffs predicted to shrink, such that narrow beaches (<50 m width) may disappear under 1-m SLR. As a standalone tool, ShoreTrans is transferable to many coast types and will provide coastal practitioners with a simple first-pass estimate of how the 2D appearance of a complex profile may change under SLR. A future benefit will be to combine this approach with existing hybrid modelling techniques to augment SLR translation predictions.

1. Introduction

Coasts are amongst the most densely populated regions on the planet and predicting how coastlines will respond to accelerating sea level rise (SLR) over coming decades is one of the primary challenges facing the field of coastal research. Sandy shores make up one-third of the world's coastlines and one-quarter of these may be eroding under present low rates (<5 mm/yr) of SLR (Luijendijk et al., 2018; Mentaschi et al., 2018). Under accelerated rates of SLR, shorelines globally are likely to recede landward without significant nourishment (Dean and Houston, 2016), which will be mitigated locally by isostatic rebound or positive sediment budgets, with SLR itself acting to modify sediment budgets in some settings (Fruergaard et al., 2015, 2021). On natural, unmodified coastlines, with ample sediment availability, the shoreface will in most

* Corresponding author.
E-mail address: jak.mccarroll@plymouth.ac.uk (R.J. McCarroll).

https://doi.org/10.1016/j.margeo.2021.106466
Received 19 September 2020; Received in revised form 4 February 2021; Accepted 10 March 2021
Available online 16 March 2021

instances be translated upward and onshore (e.g., Bruun, 1954), maintaining beach width. By contrast, on hard-engineered or rocky coastlines, where seawalls or cliffs bound the back of the beach, or where infrastructure such as housing or roads restrict onshore translation, then SLR may lead to the disappearance of beaches by the end of the century (Vitousek et al., 2017a; Vousdoukas et al., 2020). SLR and associated coastal recession will also exacerbate the frequency and severity of extreme events such as coastal flooding (Vitousek et al., 2017b), and the erosional and direct structural impacts of extreme storms (Masselink et al., 2016).

Longer-term (decadal to centennial) shoreline changes result from mutual feedback between the coastal profile, sediment budget (Rosati, 2005; Dean and Houston, 2016), wave climate (e.g., Kinsela et al., 2016), and rate of sea level change; noting that in this paper, we only discuss sea level *rise*. The most commonly used approach for estimating SLR profile translation is the Bruun rule (Bruun, 1954), which assumes the active profile is shifted upward and onshore with rising sea level, eroding the beach and dune, and accreting the lower part of the profile, through purely offshore sediment transport (details in Section 3). The Bruun rule has been heavily criticised (e.g., Cooper and Pilkey, 2004; Ranasinghe et al., 2012; Cooper et al., 2020), yet is still extensively used in many applications in coastal processes research (e.g., Vousdoukas et al., 2020). At longer timescales (centennial to millennial), shoreline changes are increasingly a function of the hinterland surface gradient (Wolinsky and Murray, 2009), substrate slope and distance of translation. We restrict our analysis to $\leq$100 years, where sediment budget and SLR are the dominant controls.

Morphodynamic modelling of future coastlines comes in a variety of forms (we adopt the terminology of Ranasinghe, 2020). Process-based 2D-horizontal and 3D models are now being shown to be capable of multi-decadal simulations (Luijendijk et al., 2019) provided sophisticated down-scaling techniques are applied. Yet, such approaches are generally resource intensive, limiting their use to smaller spatial and temporal domains. 'Bottom-up' physics based morphodynamic models are also subject to significant error when run over longer periods due to presently unresolvable sediment transport processes (a form of epistemic uncertainty) which must be crudely parameterised (Robinet et al., 2018).

Recent efforts have been to move towards 'hybrid' or 'reduced complexity' models (Ranasinghe, 2020), that are modular in nature (using elements of process-based, equilibrium and data-driven models), and are typically built for speed, for example to assess global coastlines (e.g., Vousdoukas et al., 2020) or to include large probability distributions to assess uncertainty (Le Cozannet et al., 2019; Toimil et al., 2020). Combined one-line 'cross-shore, longshore' models which may or may not include SLR (e.g., Toimil et al., 2017; Vitousek et al., 2017a; Robinet et al., 2018, 2020; Antolínez et al., 2019) offer a fast, convenient alternative to process-based models that can be used to assess larger regions (100's km) at decadal-centennial timescales. The longshore transport component of these models is generally a pre-existing longshore transport equation (e.g., 'CERC' formula; USACE, 2002). The cross-shore component is typically based on a shoreline equilibrium model (e.g., Davidson et al., 2010; Montaño et al., 2020). For SLR translation, PCR (Ranasinghe et al., 2012) is a process- and probability-based profile change model that offers an alternative to Bruun-type translation by estimating dune erosion under raised sea level, scaling with beach slope and run-up, and could potentially be incorporated into other reduced complexity models. However, many reduced complexity models opt for the simplicity and speed of the Bruun rule (e.g., Toimil et al., 2017) or variants thereof (Antolínez et al., 2019), which effectively collapses cross-shore profile information down to a single value, potentially neglecting important controls on profile change. Therefore, a critical next step in improving regional-scale, multi-decadal prediction of shoreline change is to synthesize recent achievements in reduced complexity shoreline models and combine them with a 2D profile evolution model that addresses some of the problems of the Bruun rule (e.g., the assumption of purely offshore transport and not accounting for accommodation space), yet is still simple and fast enough for broad-based, rapid assessments.

This niche may be filled by simple, rules-based, translation models, which assume an 'active profile' or 'time-invariant' upper shoreface. 'Time-invariant' in this instance implies that the upper section of the profile will maintain its height and shape, when averaged over a period of several years, and can react rapidly relative to SLR by translating vertically and horizontally, while also noting that the height of this active profile may vary depending on time-scale (Cowell and Kinsela, 2018). Translation models typically parameterise the geometry of the shoreface profile, for example using the power function of Dean (1977). The Shoreface Translation Model (STM) of Cowell et al. (1992, 1995, 2003a,b) applies a given SLR and solves numerically to conserve volume. Another translation model (Stive and De Vriend, 1995), parameterises profile geometry and adds a simple cross-shore transport formulation to the lower shoreface. There are also examples of process-based (i.e., physics-driven) models which achieve similar results in modifying the shoreface at geological timescales (e.g., Storms et al., 2002), though these are likely to be too complex to be inserted into a hybrid/reduced complexity approach. Profile translation models are extremely useful in providing a fast estimate of the future shoreline change envelope, potentially encompassing both trend changes and short-term variability, and can be used to test the impact of uncertainty by applying probability distributions to input variables to determine a probabilistic distribution of outcomes (Cowell et al., 2006).

Two recent flume-based studies tested simple translation models against observed laboratory data (Atkinson et al., 2018; Beuzen et al., 2018), determining that an effective technique for estimating SLR impacts on complex profiles was to algorithmically raise the existing profile, then iteratively shift it onshore until volume is conserved. For wall-backed profiles (Beuzen et al., 2018), the profile is translated onshore as if the wall were not present, then the hypothetical erosion demand behind the wall is transferred offshore of the wall, potentially reducing beach width.

The application of translation models has been fairly limited in determining SLR impacts. Recent examples of the translation approach include Kinsela et al. (2017), who used a volumetric approach with implicit profile translation to include short-term variability (storm erosion) and sediment budget components external to profile response, while Wainwright et al. (2015) showed the benefits of using both a translation model for long-term change and a joint-probabilistic storm erosion model for assessing short-term variability. Erikson et al. (2017) developed a method for translating profiles with and without cliffs, with similarities to the method we introduce here.

Here we present a simple shoreface translation tool (ShoreTrans) intended for rapidly testing hypotheses on coastal change over periods of ~10 to 100-years, based on user inputs for sediment budget components (Fig. 1) and an assumption of an active profile that is maintained through time. ShoreTrans is based on the translation approach of Atkinson et al. (2018) and Beuzen et al. (2018) and the budgeting method of Dean and Houston (2016), using the surveyed profile for translation (e.g., Erikson et al., 2017; Kinsela et al., 2017), as opposed to the numerical approximation of earlier approaches (e.g., Cowell et al., 1995; Stive and De Vriend, 1995; Masetti et al., 2008; Wolinsky and Murray, 2009). This is a key difference as it allows for high-resolution, site-specific features, such as irregularly shaped dunes, non-erodible substrate, and structures. We introduce two long-term monitoring locations in the UK: Perranporth Beach and Start Bay (Section 2), that will act as demonstration sites for the model. The translation and budgeting methods are then described in detail (Section 3), accounting for various morphologic features and processes, including: seawalls, cliffs, dunes, bedrock substrate, short-term variability, as well as other sources and sinks. The tool incorporates probabilistic uncertainty, using Monte Carlo simulations and probability distributions according to previously established methods (Cowell et al., 2006; Kinsela et al., 2017).

ShoreTrans is then applied to assess potential shoreface translation and sediment budgets at the two demonstration sites (Sections 4 and 5). A conceptual approach demonstrating sensitivity in shoreline recession to varying inputs is introduced along with discussion and limitations in Section 6, and conclusions in Section 7.

2. Demonstration sites

The shoreface translation and budgeting tools to be introduced in Section 3 are intended to be broadly applicable across a large range of coast types; however, this first iteration of the model has been motivated and designed based upon two UK macrotidal sites that exhibit a diverse range of shoreface types: (i) Perranporth, a high-energy, cross-shore dominated sandy embayment; and (ii) Start Bay, a moderate energy, alongshore dominated embayment, with multiple gravel barrier sub-embayments separated by small headlands, and a range engineering interventions along the shoreline. Although both sites are macrotidal, the translation approach is applicable to any tidal regime, with tide acting as a control on inputs to the model (e.g., bed slope), but not a direct input itself. Certain coastal types are not covered by the demonstration sites and are not included in this iteration of the ShoreTrans tool, e.g., soft rock cliffs (see Limitations, Section 6.3). Brief site description are given below (Sections 2.1 and 2.2), with more detailed site information, including time series of shoreline evolution, presented in the context of the modelling results (Sections 4 and 5).

2.1. Site 1: Perranporth Beach

Perranporth Beach, Cornwall, UK (Fig. 2a-d) is a 3.5-km long, sandy, high-energy beach (annual mean $H_s = 1.6$ m and $T_p = 10$ s), with a wide dissipative shoreface and active double-bar morphology covering the low-tide region to the inner-subtidal. The beach is backed at the south end (Fig. 2b) by dunes (foredune height of 6–8 m), at the mid-beach (Fig. 2 c) by large cliffs (>50 m height), and at the northern end (Fig. 2d) by perched dunes (foredune height 10 m) that rise steeply inland (~15°), overlaying bedrock cliffs that outcrop in some areas. Mean grain size (D_{50}) is medium sand, with 0.33 mm on the upper beach, 0.48 mm at Mean Low Water Springs (MLWS), fining to 0.30 mm from 22 to 26 m water depth (Valiente et al., 2019a). Tidal regime is macrotidal with mean spring tide range > 6 m. A limited section at the south of the beach has been extensively studied since 2006 (e.g., Poate et al., 2014; Stokes et al., 2015; Scott et al., 2016), beach profile surveys (Fig. 2b-d) indicate an annual oscillation in intertidal volume, with periodic extreme events that take multiple years for recovery (5–7 years). Initially, the system was inferred to be near-closed, with cross-shore storm-recovery processes dominating the transport budget. Only since 2016 has the sediment budget of the entire embayment been thoroughly studied (Valiente et al., 2019a; Valiente et al., 2019b), determining, unexpectedly, that the subtidal budget is open, likely due to highly energetic longshore (headland bypassing) and cross-shore processes (mega-rips) operating at significant depth (Valiente et al., 2019b; McCarroll et al., 2018; Valiente et al., 2020). The upper shoreface-dune system appears to be dynamically stable, or with a moderately positive sediment budget, with Valiente et al. (2019b) demonstrating the full-embayment system gained ~4×10^5 m^3 from 2011 to 2018 (O[10] m^3/m/yr), though with a large interannual variability and loss of sediment from the system in some multi-year periods.

2.2. Site 2: Start Bay

Start Bay, Devon, UK (Fig. 2e-h), is a 12-km long embayment, with multiple fine-gravel beaches divided by small rocky headlands (Wiggins et al., 2019). From south to north, the beaches include: Hallsands (HS in Fig. 2e), Beesands (BS), Slapton Sands (SS) and Blackpool Sands (BK). Slapton Sands is the longest beach, at >4 km length, with a narrow (100–200 m wide) and low (~5–7 m above mean sea level) barrier that is backed by a lagoon and has a road constructed along the crest. Across other sections of the bay, the barrier backs onto wetlands and slate to schistic cliffs. Built-up areas, including the villages of Torcross (at P0 in Fig. 2e) and Beesands, are heavily defended, with rock-armour and seawalls protecting buildings that would otherwise fall within the active shoreface. All barriers are comprised of fine gravel, with a transition to sand at ~10 m water depth (Hails, 1975). Given that the barrier is pure gravel and the lower shoreface is shelly sand, it is a reasonable assumption that there is no exchange between the upper and lower shoreface. Wave heights are generally low (< 1 m), apart from during storm events (H_s up to 5 m). The wave climate is bi-directional, with dominant swell waves from the SW refracted over Skerries Bank (McCarroll et al., 2020) into the bay, driving northward transport, and less frequent short-period easterly events, driving southward flux. Tidal regime is meso-macro tidal, with a 4.3 m mean spring range.

Rates of longshore transport have been extensively studied at Start Bay, and the system has been found to be closed to the south of Hallsands and north of Blackpool Sands (Wiggins et al., 2019). A long-term (>100 years) south to north longshore transport trend may have contributed to the destruction of Old Hallsands, a fishing village just south of present day Hallsands (HS in Fig. 2e; Wiggins et al., 2017; McCarroll et al., 2020), in addition to the impact of aggregate dredging of the shoreface in that area at the time. Short-term changes in longshore flux, forced by variations in the bi-directional wave climate, result in rapid changes in beach width due to rotation (Wiggins et al., 2019; McCarroll et al., 2019a), particularly near headlands (e.g., Fig. 2f). Beach profile surveys conducted regularly since 2007 (Fig. 2f-h) indicate that shorelines along the southern two-thirds of the bay are receding at up to 1 m/yr (Fig. 2f, g), northern Slapton Sands is accreting at up to 1 m/yr (Fig. 2h), while the far-northern Blackpool Sands profiles are rapidly accreting at up to 1–5 m/yr, much of which is due to northward headland bypassing and 'full embayment rotation' during the exceptional 2013/14 winter (Wiggins et al., 2019).

3. Description of the shoreface translation and sediment budgeting tool

A sediment budget approach (Fig. 1) to determine change in shoreline position (Eq. 1, ΔX, taking positive as offshore) applied either to a single cross-shore transect, multiple transects (the approach taken in this study), or an alongshore averaged transect, can be simplified to four elements: (i) profile translation due to SLR; (ii) sediment flux in the cross-shore between the backbarrier, upper (active) shoreface and lower shoreface; (iii) sediment gains and losses due to alongshore transport gradients; and (iv) other gains and losses, e.g., profile dredging/nourishment, biogenic carbonate production and exchange with estuaries.

$$\Delta X = f_{SLR} + f_{cross-shore} + f_{longshore} + f_{\{sources,sinks\}} \quad (1)$$

For this approach, the concept of the 'active profile' is important (Stive and De Vriend, 1995). The active profile is defined as the section of the profile assumed to adjust rapidly to incident wave conditions, much faster than the rate of profile translation due to SLR. Under this assumption, the active profile is assumed to be in equilibrium with forcing when averaged over several years or more, maintaining a fixed shape. Using the approach of Cowell et al. (1995), the upper limit of the active profile is defined as the dune toe for profiles with large dunes, and the crest of the barrier for low barrier profiles. The lower limit of the active profile (defined as Z_{D1}, Fig. 1) is more difficult to define. Cowell and Kinsela (2018) suggest the active profile lower limit should lie between the depth of observable change on an annual basis ('*depth of closure 1*', or DoC_1) and the depth below which no significant net cross-shore transport by waves affects profile shape (DoC_2). Both DoC_1 and DoC_2 may be estimated from Hallermeier (1981).

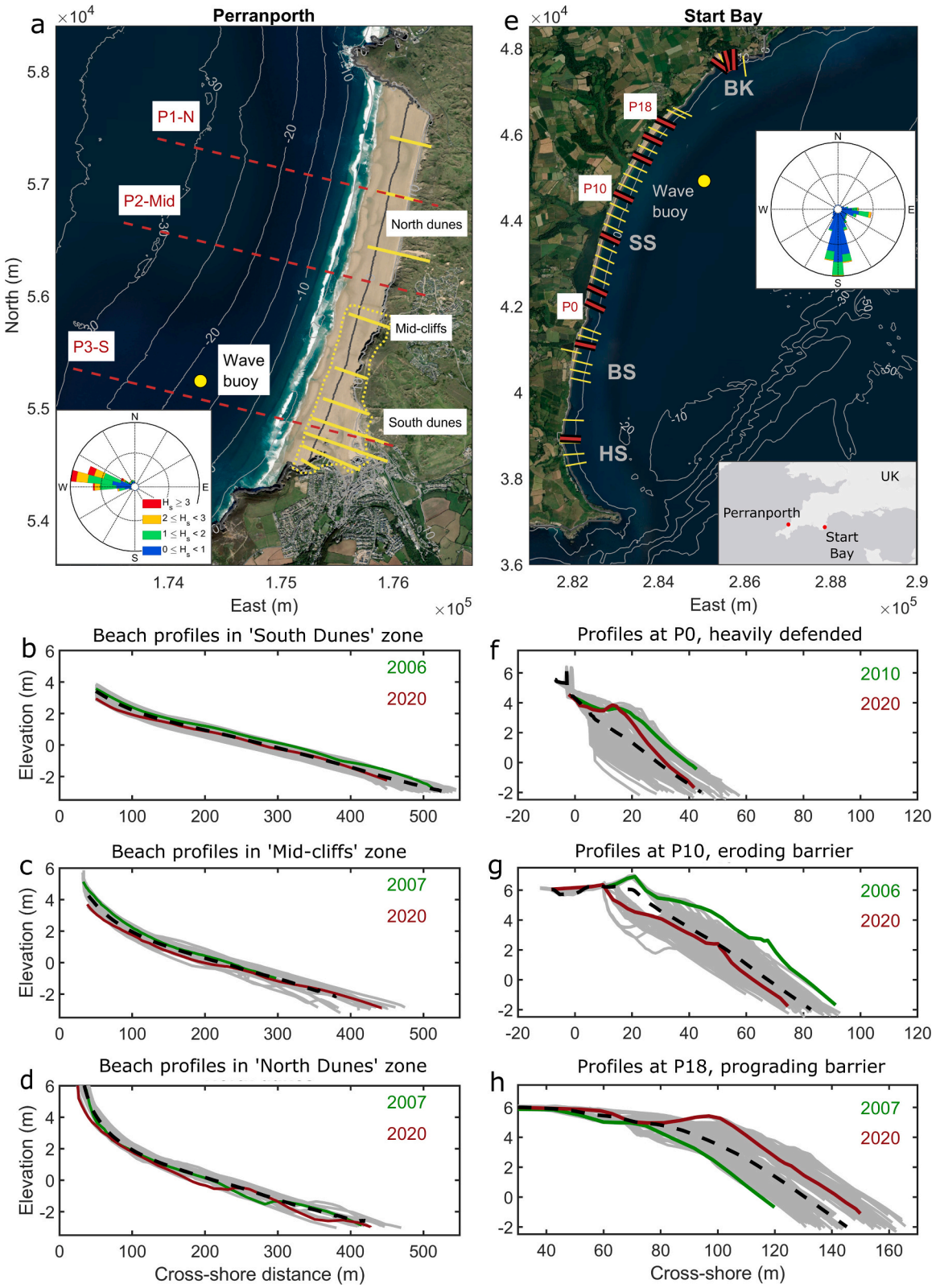

Fig. 2. Demonstration sites. First column: (a) Perranporth map with wave rose, showing survey lines (Plymouth Coastal Observatory, solid yellow), southern 3D-survey area (University of Plymouth, dotted yellow), and transects that will be used for the model application (dashed red lines); (b) beach profiles in front of the south dunes, alongshore averaged from southern 3D-survey area; and (c-d) beach profiles in front of mid-beach cliffs and north dunes respectively. Second column: (b) Start Bay map with wave rose, survey profiles (University of Plymouth and Plymouth Coastal Observatory, yellow) and transects selected for model application (red); (f-h) are profile envelopes for selected profiles along Slapton Sands. For Start Bay, sub-embayments include: Hallsands (HS), Beesands (BS), Slapton Sands (SS), and Blackpool Sands (BK). All elevations are in Ordnance Data Newlyn (ODN), with 0 m ODN approximately equal to mean sea level. (For interpretation of the references to colour in this figure legend, the reader is referred to the web version of this article.)

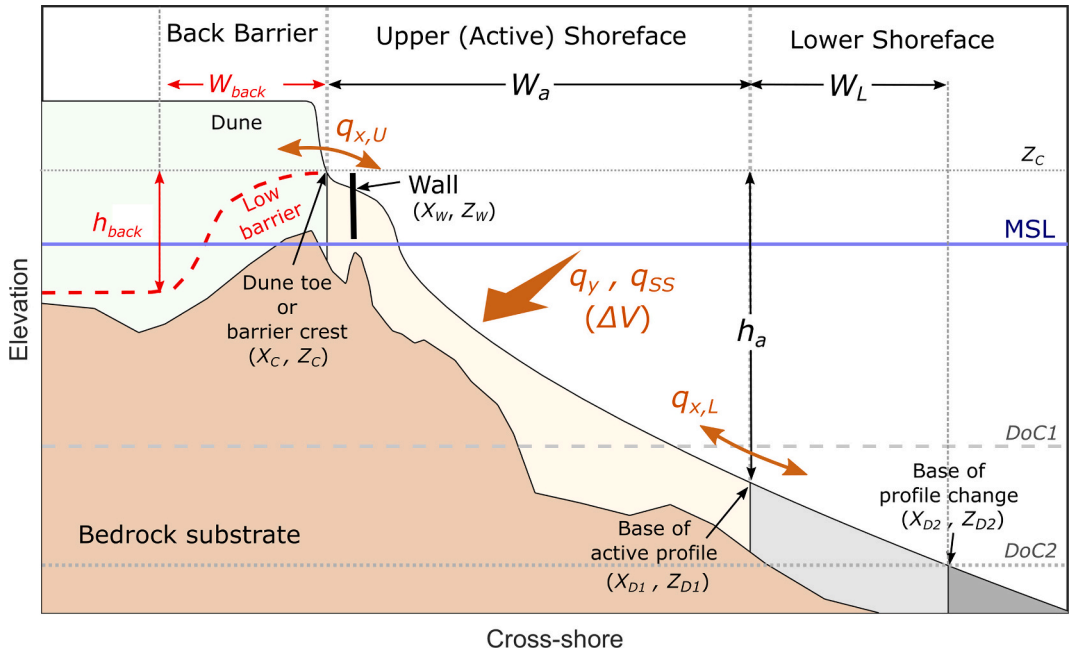

Fig. 1. Components of the ShoreTrans model.

$$DoC_1 = 2.28\,H_{12,t} - 68.5\left(\frac{H_{12,t}^2}{gT_t^2}\right) \quad (2)$$

and

$$DoC_2 = \left(\overline{H_{s,t}} - 0.3SD_s\right)\overline{T_{s,t}}\left(\frac{g}{5000D_{50}}\right)^{0.5} \quad (3)$$

where $H_{12,\,t}^2$ is the significant wave height exceeded for 12 h per t years, T_t is the associated peak period, $\overline{H_{s,t}}$ is annual significant wave height, SD_s is the wave height standard deviation, $\overline{T_{s,t}}$ is the time-averaged wave period and D_{50} is the median grain size. As the response rate of the lower shoreface (Anthony and Aagaard, 2020) is expected to decrease with increasing depth, faster rates of SLR will result in a shallower active shoreface extent (Cowell and Kinsela, 2018; Eqs. 2, 3), with a potential hysteresis period of 'catch-up' after an initial phase of SLR, where the lower shoreface gradually adjusts to the new equilibrium sea level, potentially over 1000's of years (e.g., Kinsela et al., 2016; Daley and Cowell, 2012).

We adopt a range of Z_{D1} from a shallow limit of $Z_{D1} = -DoC_1$ to the mid-way point between DoC_1 and DoC_2, taking $Z_{D1} = -(DoC_1 + DoC_2)/2$. This is broadly consistent with Cowell and Kinsela (2018), who show that, for rapid SLR, Z_{D1} will become shallower and approach $-DoC_1$. Given our application will be to relatively high rates of SLR (~1 cm / year), we assume Z_{D1} will fall in the upper half of the range between $-DoC_1$ and $-DoC_2$. However, many authors tend to use the shallower limit (i.e., $Z_{D1} = -DoC_1$; e.g., Robinet et al., 2020; Vousdoukas et al., 2020). The point below which no significant bed change occurs (at the timescale of interest) is defined as $Z_{D2} = -DoC_2$, also consistent with Cowell and Kinsela (2018), acknowledging that net transport may occur below this depth over longer time periods (100 s to 1000's years).

Sediment fluxes (in m^3/m/yr) to the profile controlling volume (Fig. 1, orange arrows) include: (i) cross-shore flux between the upper and lower shoreface [$q_{x,\,L}$]; (ii) cross-shore flux between the active profile and backbarrier [$q_{x,\,U}$], (iii) net flux into the profile from long-shore transport gradients [$\Delta q_y = q_{y,\,updrift} - q_{y,\,downdrift}$]; and (iv) flux from other sources and sinks [q_{ss}]. Taking a simplification of the Exner equation (Wolinsky, 2009), using a form similar to Dean and Houston (2016), the sediment budget approach in (Eq. 1) can be applied as a rate

$$\frac{dX}{dt} = -\frac{dS}{dt}\left(\frac{W_a}{h_a}\right) + \frac{1}{h_a}\left(q_{x,U} - q_{x,L} + \Delta q_y + q_{ss}\right) \quad (4)$$

where t is time, X (m) is the shoreline position (positive offshore), S (m) is sea level, h_a (m) is the active profile height and W_a is the active profile width (Fig. 1). Using a positive offshore frame of reference, an onshore (negative) flux from the lower to upper shoreface ($-q_{x,\,L}$), produces a positive change in shoreline positive. Additionally, we express along-shore flux simply as a net rate of input to the control volume, as opposed to a longshore transport gradient.

In (Eq. 4), the SLR translation component is the standard version of what is commonly referred to as the 'Bruun rule' (Bruun, 1954; Bruun, 1962; Bruun, 1988), which can be expressed as a rate (as per Eq. 4), or a time-integrated extent of shoreline translation:

$$\Delta X_{Bruun} = -\Delta S\left(\frac{W_a}{h_a}\right) \quad (5)$$

where ΔX_{Bruun} is the shoreline change due to SLR. The standard Bruun rule assumes that the active profile will be raised by ΔS and will shift onshore to balance total volume, with shoreline recession equal to the magnitude of SLR divided by the profile gradient. Later iterations (e.g., Kriebel and Dean, 1993; Cowell et al., 1995) demonstrated that the elevation of the dune toe or the crest of barrier (Z_C, Fig. 1) is more appropriate for realistic profiles than using an idealised berm height.

The standard Bruun rule (Eq. 5) assumes SLR translation will occur through purely offshore flux, such that the upper part of the active profile will be eroded while the lower part of the active profile will accrete. This assumption is violated in the case of overwash and rollback of low barriers (Rosati et al., 2013), where onshore transport from the active profile to the backbarrier can be observed, and therefore the standard Bruun rule will underestimate recession magnitude. A more generalised approach (Dean and Maurmeyer, 1983) is

$$\Delta X_{Bruun,Gen} = -\Delta S\left(\frac{W_a + W_{back}}{h_a - h_{back}}\right) \quad (6)$$

where h_{back} is the depth of closure or base of beach sediment in the

lagoon backing the barrier and W_{back} is the width of the back barrier (Fig. 1). The standard Bruun rule (Eq. 5) is an end-member instance of the general rule, in which case $W_{back} = 0$. Applying (Eq. 2) and (Eq. 3), recession rates will be lower for erodible dune-backed beaches (offshore transport) and higher for barriers that rollover (onshore transport). This can be shown along a continuum of profile shapes (Cowell et al., 2006) and has been generalised to account for longer time periods, with varying underlying substrate morphology (Wolinsky and Murray, 2009).

Eq. (4) can be integrated over time to a total amount of shoreline change, with the flux terms now expressed as total volume change per metre alongshore (m^3/m),

where subscripts for each volume component match (Eq. 4) and ΔX_{SLR} may use any method for profile translation due to SLR, e.g., (Eqs. 5,6) or an algorithmic method such as the ShoreTrans approach that will be described subsequently. For the ShoreTrans application, (Eq. 7) is segregated into: (i) cross-shore fluxes to the backbarrier or lower shoreface that modify the profile shape, but not the total profile volume [ΔV_x terms in Eq. 7]; and (ii) longshore transport inputs and other sources/sinks, that do modify the total profile volume [ΔV_y, ΔV_{ss} terms in Eq. 7]:

$$\Delta X = \Delta X_{SLR} + \underbrace{\frac{\Delta V_{x,U} - \Delta V_{x,L}}{h_a}}_{\text{Cross-shore flux.No change to total profile volume}} + \underbrace{\frac{\Delta V_y - \Delta V_{ss}}{h_a}}_{\text{Longshore flux\&sources/sinks.Gains/losses to total profile volume}} \quad (7)$$

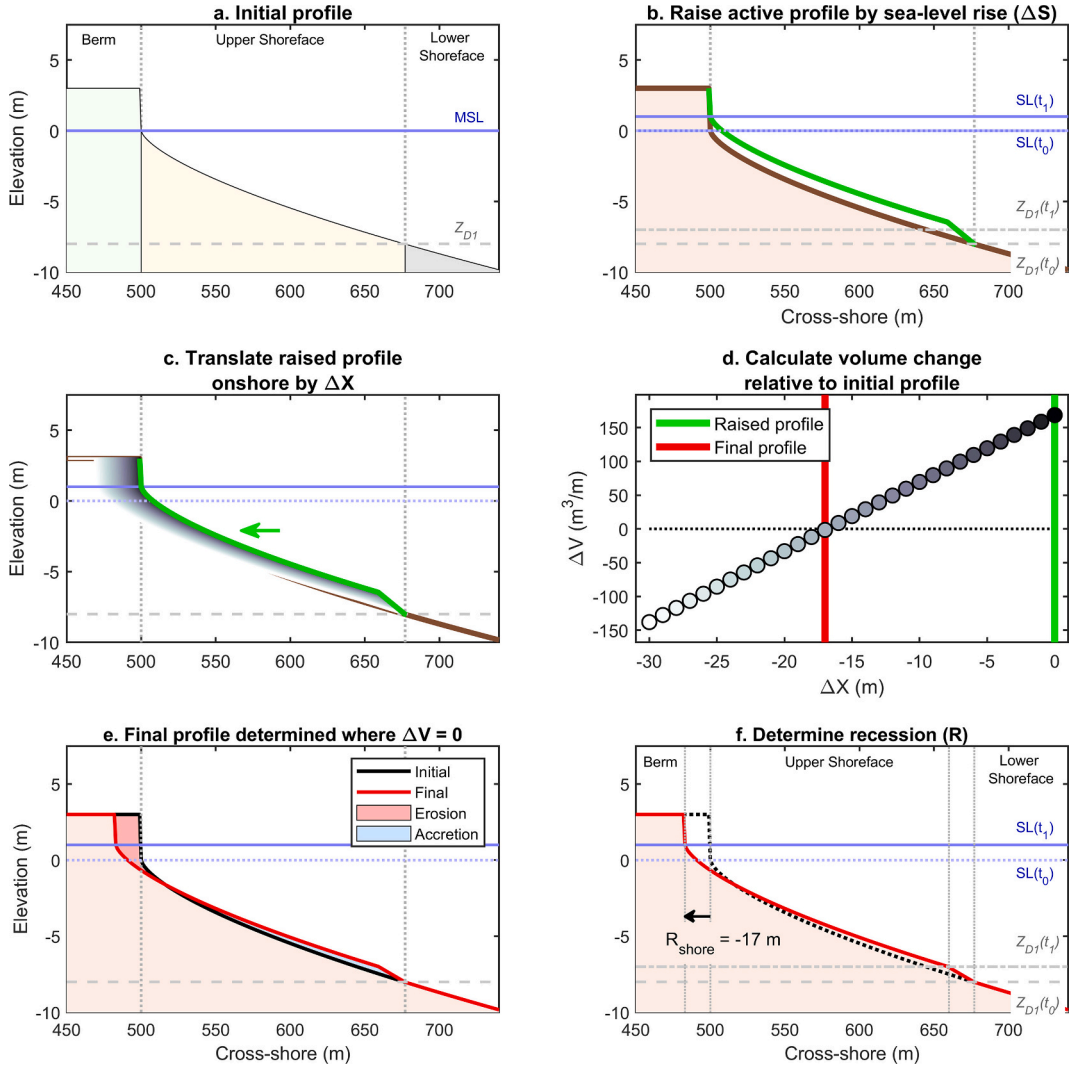

Fig. 3. Active profile translation example using a Bruun-like profile, following the method of Atkinson et al., 2018. The initial profile (a) is raised by ΔS (b), then is translated onshore, shown in section view (c) and as a function of change in shoreline against change in volume (d), with an optimization routine used to minimise ΔV_{error} (Eq. 9). For this example, the target volume change is zero ($\Delta V = 0$; Eq. 9), with the final profile in (e), and recession determined in (f). The shading in (c, d) are an example envelope of translated profiles, from $0 < \Delta X \leq 30$ m.

3.1. Profile translation

The basic mechanism of the translation model is to shift the active profile (Fig. 3a) up by the change in sea level (ΔS; Fig. 3b) and shift onshore (Fig. 3c) to the point at which net volume change is zero (as per Atkinson et al., 2018; Fig. 3d-e). The translation tool requires at a minimum, a cross-shore profile (x_i, z_i).

$$z_i(x_i, t_1) = z_i(x_i - \Delta X, t_0) + \Delta S(t_0 \rightarrow t_1), a < x < b \quad (8)$$

with bed elevation (z), determined at an initial and subsequent time point (t_0 and t_1). The integration bounds (a, b) represent the on- and offshore points beyond which there is no bed elevation change, and will in the basic case be the bounds of the active profile, with onshore bound ($a = X_C + \Delta X$), and offshore bound ($b = X_{D1} + \Delta X$), but this may vary depending on inputs (described in subsequent sections). For points onshore of a and offshore of X_{D1}, the profile is unchanged ($z_{t1} = z_{t0}$). Points between b and X_{D1} are linearly interpolated across. The point at the base of the active profile [X_{D1}, Z_{D1}] is held constant for a given time-step.

To solve for ΔX, (Eq. 8) is substituted into (Eq. 9) and solved algorithmically with an optimization routine (Fig. 3c-d show a full range for translation distances for illustration), conserving volume (i.e., minimizing ΔV_{error}). A fixed cross-shore resolution of 1-m is used in all applications, resulting in maximum volume rounding errors approximately half the height of the active profile (~10 m^3/m).

$$\Delta V_{error} = \int_a^b (z_{t1} - z_{t0})dx + \Delta V \quad (9)$$

Changes to total profile volume occur due to longshore inputs and other sources and sinks ($\Delta V = \Delta V_y + \Delta V_{ss}$; see Eq. 7). All volume integrations are conducted above a base of profile change (Fig. 1; Z_{D1} for the basic case, and Z_{D2} where there is sediment flux between the upper and lower shoreface, described in Section 3.4). This approach can be applied to three basic scenarios: (i) a change in sea level with no change in total volume [$\Delta S \neq 0$; $\Delta V = 0$]; (ii) a change to profile volume without sea level change [$\Delta S = 0$; $\Delta V \neq 0$]; or (iii) change to both sea level and total volume [$\Delta S \neq 0$; $\Delta V \neq 0$].

For a case with uniformly offshore transport and all volume terms in (Eq. 7) equal to zero, solving for ΔX using (Eqs. 8,9) will give the same result as the Bruun rule, with the translation distance equal to shoreline recession ($\Delta X = R_{shore}$; Fig. 3f). Rules described in subsequent sections will result in ΔX varying from the Bruun rule, potentially changing the shape of the profile (where $\Delta X \neq R_{shore}$), e.g., in front of a sea-wall.

3.1.1. Step-smoothing at the base of translation

Applying a Bruun-style translation can result in a large unrealistic step at the base of the active profile, particularly when the onshore translation distance is short relative to SLR. To avoid this, a linear interpolation is made from the base of the active profile (X_{D1}, Z_{D1}) to a point onshore in the translated profile, with a minimum span of ΔX or 10% of the active profile width (whichever is larger), Fig. 3b shows an example. Similarly, for prograding profiles ($\Delta X > 0$), a step will occur at X_{D1}, which is removed by applying a linear interpolation from the top of the step [$z_{t1}(X_{D1})$] extending offshore to the initial profile [$z_{t0}(X_{D1} + \Delta X)$], Section 3.4 (Fig. 7a) gives an example. The latter allows for a small amount of sediment to be transported beyond the base of the active profile. The approach here is to avoid clearly unrealistic profile shapes, while trying to maintain consistency with existing rules and approaches. Offset issues may also occur when determining the top of the active profile, as the beach terminates at a seawall or merges into dunes, and these factors are addressed in Sections 3.2 and 3.3.

3.2. Profile translation involving seawalls, cliffs and underlying non-erodible substrate

Erosion demand on the upper profile under SLR has been found to be similar for profiles with and without seawalls (Beuzen et al., 2018). However, where a wall is present, the potential erosion onshore of the wall, were it not present, is transferred offshore to the area adjacent to the wall, concentrating erosion in the vicinity of the wall, demonstrated in Fig. 4a-c. The 'wall effect' is determined by initially translating the profile as if the wall was not present (solving for ΔX in Eqs. 8,9). The 'wall demand' volume is:

$$\Delta V_{wall} = \int_a^{X_w} (Z_W + \Delta S) - z(x, t_1)\, dx \quad (10)$$

as indicated in Fig. 4b, defined by subtracting the translated surface [$z(x, t_1)$] from the rectangular block capped by the elevation of the toe of the active profile at the base of the wall (Z_W in Fig. 1 and Fig. 4a) plus the change in sea level (ΔS). The wall location is specified as a cross-shore location (X_W) or the elevation of the surface profile at which the wall occurs (Z_W). 'Walls' in the translation model may include hard-rock cliffs or cliffs buried under perched dunes. The height of the wall and the shape of the profile behind the wall have no impact on the ΔV_{wall}.

The wall demand volume is then distributed in front of the wall in a triangular wedge, with maximum additional bed level at the base of the wall (ΔZ_{WR}, "WR" is for wall redistribution), linearly tapering to zero at a distance ($X_{wall} + \Delta X_{WR}$). Total profile volume is conserved in all cases. The distance ΔX_{WR} is inferred to have a default value of 1/3 the extent of

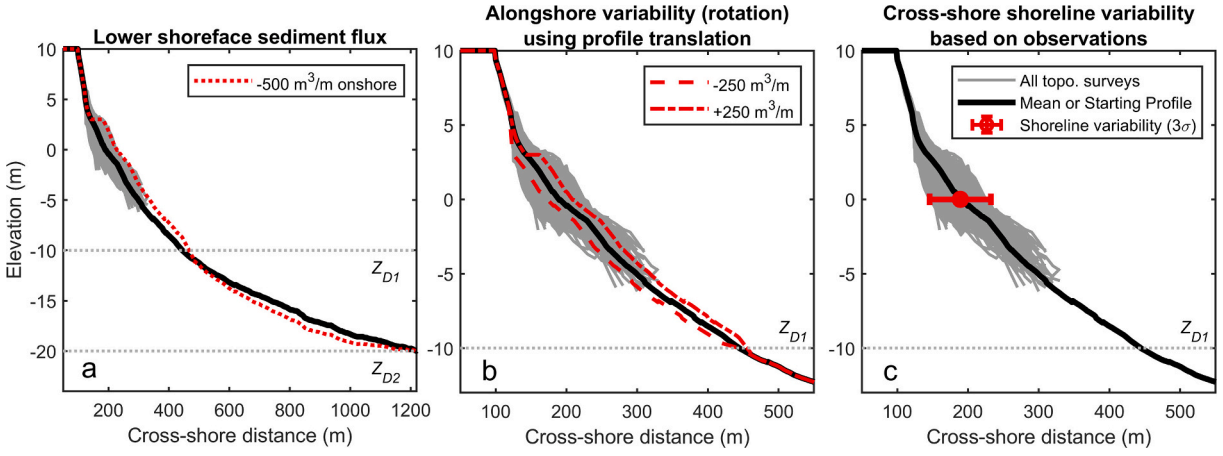

Fig. 7. ShoreTrans methods using Narrabeen (profile P4) as a demonstration. (a) long-term flux from the lower- to upper shoreface; (b) hypothetical rotation bounds; (c) use of observations to determine shoreline variability.

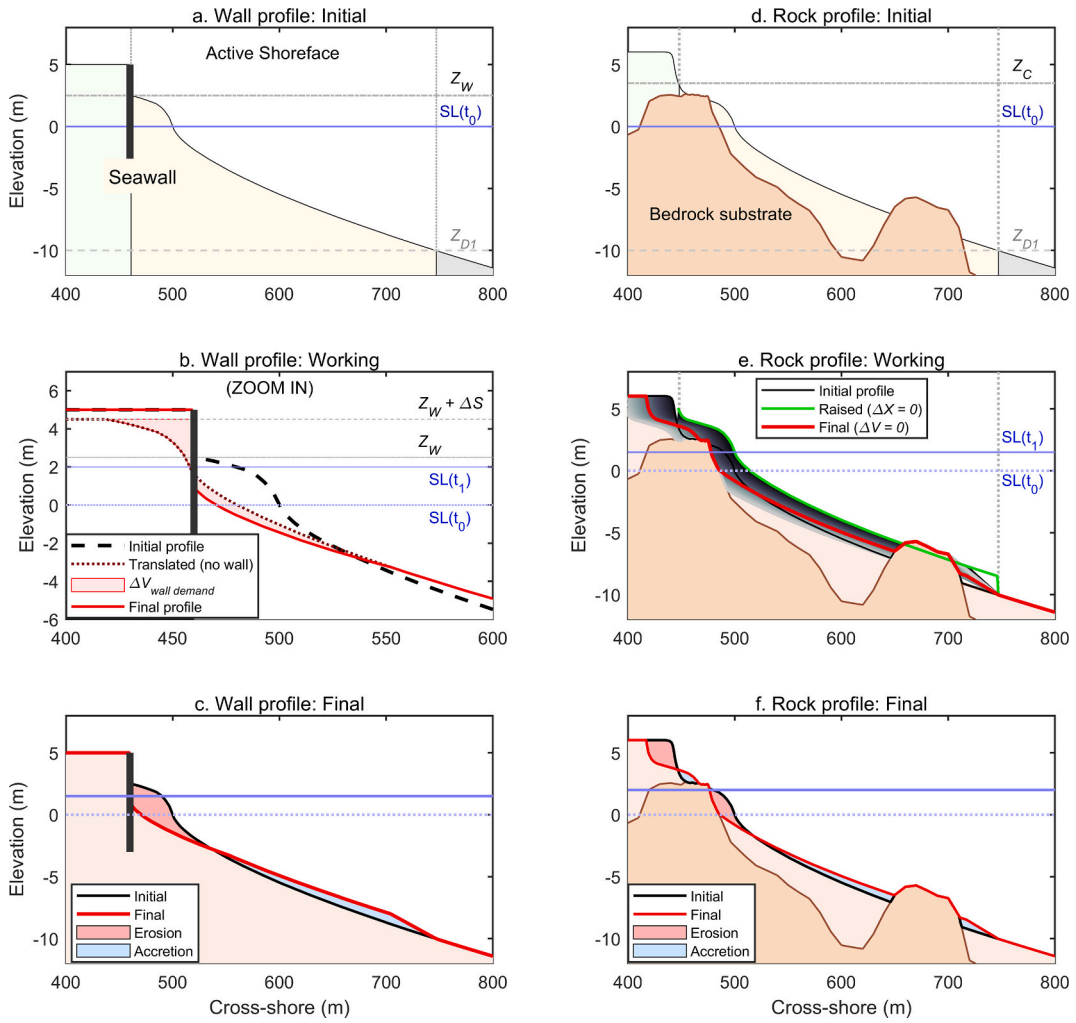

Fig. 4. Profile translation method for profiles backed by hard structures and cliffs ('walls', left column) and non-erodible substrate ('rocks', right column). The greyscale shaded area in (e) represents the envelope of translation distances, $0 < \Delta X \leq 50$ m.

the active profile based on the conceptual model of Beuzen et al. (2018) but can be modified manually. This approach requires future field validation, though is considered acceptable for an exploratory sediment budgeting tool.

$$\Delta Z_{WR} = \frac{2\Delta V_{wall}}{\Delta X_{WR}} \tag{11}$$

Persistent loss of sediment due to a negative sediment budget or large levels of SLR on a wall-backed profile may lead to severe erosion, and the disappearance of the sub-aerial beach. Left unchecked, the entire profile will erode to the depth of the base of the active profile, which is unrealistic for most scenarios. Therefore, a manual limit can be set on how much erosion can occur by setting a minimum bed elevation value for the profile toe immediately offshore the wall. Once this limit is reached (e.g., mean low water springs), no further depletion of the profile will occur.

Non-erodible surfaces (e.g., rocky reefs and isolated outcrops) may be specified as a layer; typically, this will represent a bedrock substrate (Fig. 4, second column), but may also include sub-horizontal engineered structures (e.g., a path behind a revetment). The translation algorithm must be modified so that the erodible bed can be raised and shifted with SLR, while the non-erodible layer is kept in place. This approach is adopted from Cowell et al. (2006) and Kinsela et al. (2017). Non-erodible surfaces can fill potential accommodation space, reducing translation distances (e.g., offshore reefs), or may occupy space that is projected to be eroded, increasing translation distance. Isolated sections of rocky reef or outcrops are dealt with by applying the following algorithm:

1. Separate profile layers must be provided for the bed layer ($z[x,t]$) and a non-erodible layer ($z_{NE}[x]$). Sections of 'outcrop' exist where $z(x, t_0) = z_{NE}(x)$. An initial volume calculation is made on the pre-translation bed level surface.
2. In order to avoid translating the non-erodible surface, outcrops are linearly interpolated across, providing a temporary 'rock free' layer ($z_{RF}[x,t_0]$), this layer is then used for profile translation.
3. Outcrops of the non-erodible layer are reinserted

$$z_i(x_i, t_1) = max(z_{RF}(x_i, t_1), z_{NE}(x_i)) \tag{12}$$

and a final volume is calculated. Eqs. (8,9) are applied to balance the system volume.

3.3. Translation type: rollover and encroachment

Two end-member behaviours for translating barriers are 'rollover' and 'encroachment' (Cowell et al., 1995). Rollover is associated with low barriers and low hinterland gradients, approximated with the generalised Bruun rule (Eq. 6) and may involve only onshore transport (Rosati et al., 2013) through overwash and tidal inlet processes (flood tide delta accretion). Encroachment typically occurs with bay-barriers and mainland beaches backed by steep dunes and, if applying the

Table 1
Barrier response types.

Type	Translation	Equivalent equation
1. Barrier rollover, onshore transport	Full extent of back-barrier and active profile ($X_{back} \rightarrow X_{D1}$; Fig. 1) raised and shifted onshore.	Eq. 6
2. Dune rollover, keep up with SLR	Crest of barrier raised by ΔS and translated ($X_C \rightarrow X_{D1}$). Backslope (ϕ) is manually specified.	Eq. 13
3. Dune rollover, maintain initial height	As per Type 2. After translation, barrier crest is capped at initial level.	Eq. 14
4. Encroach barrier, offshore transport	Active profile is translated ($X_C \rightarrow X_{D1}$), but no increase in bed level is permitted onshore of X_C.	Eq. 5

standard Bruun rule (Eq. 5), will involve only offshore transport. ShoreTrans requires user-specification of the dune toe or barrier crest (X_C, Z_C in Fig. 1), depending on profile type, and manual selection of the translation type. This first iteration of ShoreTrans is intended for exploratory analysis of translation potential based entirely on user input, and will not adjust translation type based on barrier shape (see Limitations, Section 6.3).

Four options for barrier response type are included in the ShoreTrans tool (Table 1, Fig. 5), including the two end-member types ('barrier rollover' and 'encroachment' modes) and two intermediate modes where the dune migrates by rollover across the barrier complex. Each of these methods is a separate algorithmic function for determining sea level rise translation (ΔX_{SLR} in [7]). Types 1 and 4 are described by previous equations (Eq. 6 and 5 respectively). Type 2 profiles are determined by moving iteratively onshore from the crest of the barrier (recalling the cross-shore resolution is $dx = 1\ m$), where ϕ is the backslope angle, until the initial profile is intersected (Fig. 5), which becomes the onshore point of closure (a).

$$\text{Type 2}: z_i(x) = z_{i+1} - tan\phi, a \leq x_i < X_C(t_1) \quad (13)$$

Type 3 begins with the output of Type 2, then applies a cap at the initial barrier crest level.

$$\text{Type 3}: z_i(x) = Z_C, for\ a \leq x_i < X_C(t_1), where\ z_i > Z_C(t_1) \quad (14)$$

The four modes are illustrated for translation of an idealised low barrier backed by a shallow lagoon in Fig. 5. There is a decrease in recession rates from Type 1 to Type 4, with 'barrier rollover' (Type 1) recession rates a factor of 2 to 3 higher than the other types. For Type 3 (capped barrier height) the barrier can be drowned, while for Type 4 (encroachment), the barrier can be drowned and eroded entirely. For all four translation methods, volume is conserved by determining the profile translation distance (ΔX, Fig. 3d) that satisfies Eqs. (8,9).

Observations suggest all these behaviours may occur for natural barriers. In general, Type 1 'rollover' behaviour is more likely for low barriers with low substrate gradient (e.g., barrier islands in southeast US; Rosati et al., 2013), while Type 4 'encroachment' behaviour will occur with large dunes and steep substrate gradient (e.g., the embayed, duned coastline of mid-NSW, Australia; Kinsela et al., 2017). The intermediate behaviours (Type 2 and 3) were introduced upon examination of observed barrier evolution at Start Bay (e.g., Fig. 2g). The type of translation behaviour a particular barrier will exhibit under future SLR is likely to be highly uncertain, noting that barrier rollover transport is likely limited to low barriers where high-energy events, such as hurricanes, can produce overwash (Orford et al., 1995; Plant and Stockdon, 2012; Lorenzo-Trueba and Ashton, 2014; Vinent and Moore, 2015; Masselink et al., 2020). ShoreTrans does not predict which of these behaviours will occur, but instead acts as a tool to investigate the likely recession rates under different encroachment/rollover scenarios. This approach allows for investigation of uncertainty by exploring a range of potential outcomes, though it is a limitation in comparison to previous models that automatically determine translation type (see Limitations, Section 6.3).

This approach uses a number of simplifying assumptions: (i) for 'Type 2', a single angle is used to describe the shape of the back-barrier, which approximates more complex real-world back-barrier shapes (Fig. 5b); (ii) the 'Type 3' option crops the barrier elevation at the initial crest level, resulting in a 'flat-top' (Fig. 5b); and (iii) no allowance is made for fluvial sediment input from the estuarine side (see Limitations, Section 6.3).

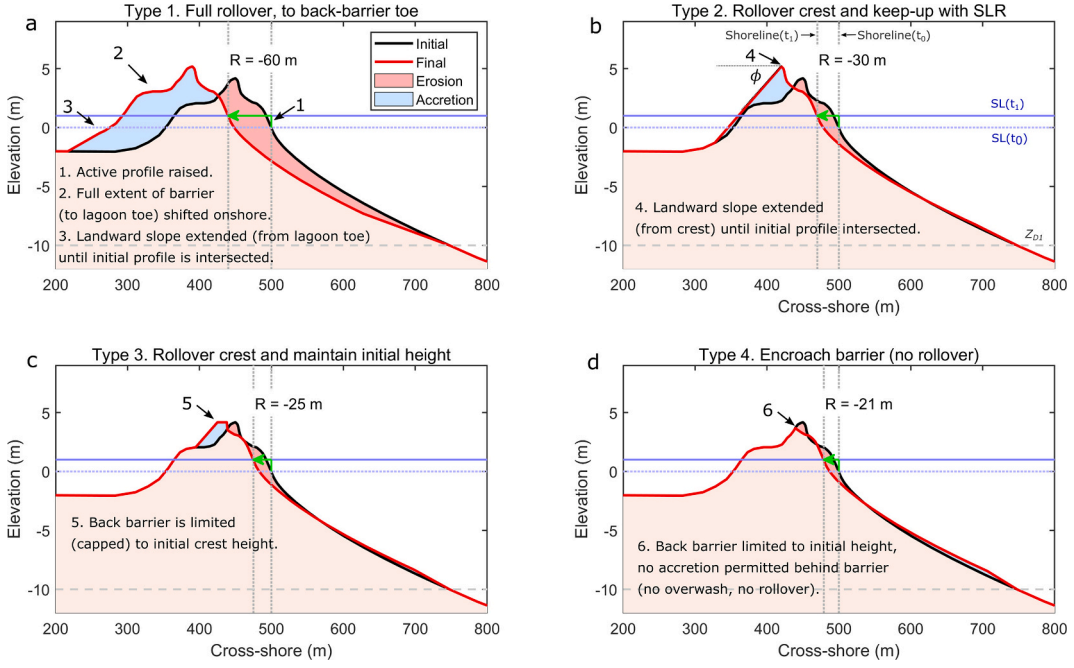

Fig. 5. Four modes of profile translation: (a) Type 1 – Full barrier rollover (b) Type 2 – Rollover and crest keep-up with SLR; (c) Type 3 – Rollover and maintain initial crest height; or (d) Type 4 – Encroachment, i.e., erode with no onshore transport beyond crest.

3.4. Cross-shore sediment fluxes with the back-barrier and lower shoreface

This section deals with cross-shore fluxes that modify the shape of the back-barrier and lower shoreface ($\Delta V_{x,\,U}$ and $\Delta V_{x,\,L}$ in Eq. 7), but do not change total profile volume.

3.4.1. Dune vertical accretion

Dune processes are complex, with recent advances occurring in process-based aeolian transport models (e.g., Hoonhout and Vries, 2016; Roelvink and Costas, 2019). The approach here is simply to incorporate a user-inputted volume flux between the beach and dune into the ShoreTrans sediment budget. Dune processes would normally occur in conjunction with 'Encroachment' style translation (Type 4, Table 1, Fig. 6). A modified 'dune accretion' profile (z_{DA}; Fig. 6a) is produced by adding a user specified volume (ΔV_{DA}) as a block of uniform height, over a specified distance (X_{DA}) onshore of the dune toe, which is likely to be site-specific, defined by extent of the foredune and changes in vegetation density

$$z_{DA}(x) = z_i + \frac{\Delta V_{DA}}{X_{DA}},\ (X_C - X_{DA}) \le x_i < X_C \tag{15}$$

The initial stage of the dune accretion process modifies the total profile volume ($V_{z,\ DA} > V_z$). The translation functions (8,9) are then applied to the interim profile (z_{DA}) to determine the translation distance (ΔX) that conserves volume. Physically, this assumes that if flux occurs

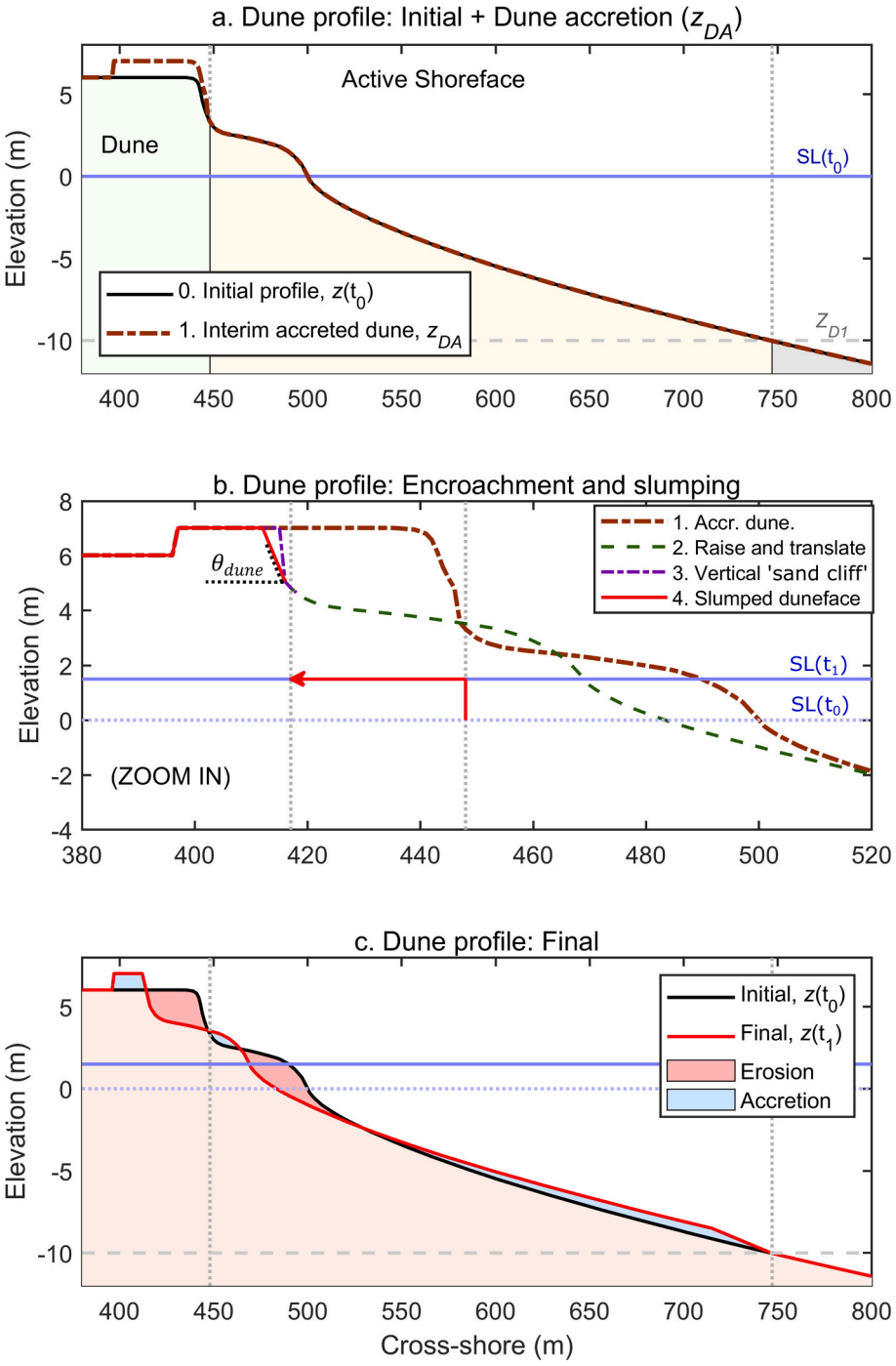

Fig. 6. Dune erosion mechanics, including (a) the initial profile, with dune accretion / shoreface accretion applied, here $\Delta V_{dune\ accretion} = 50\ m^3$ applied from the dune toe 50 m onshore; (b) the profile is raised then translated onshore (red arrow indicates magnitudes), the resulting vertical 'sandwall' is slumped to a default angle of $\theta_{dune} = 30°$; (c) the final profile is determined where $\Delta V_{total} = 0$. SL1 and SL2 are initial and final sea-level, Z_{D1} is upper depth of closure. (For interpretation of the references to colour in this figure legend, the reader is referred to the web version of this article.)

from the sub-aerial beach to the dunes, the active profile will dynamically adjust over time to maintain the initial shape, eroding the beach to conserve volume. A negative value can be used to produce vertical erosion (deflation) of the dunes. Dune accretion rates can be determined from observation or by using typical values (e.g., Stive, 2004).

3.4.2. Dune erosion and slumping

Dune erosion (Fig. 6b) is handled similarly to Kinsela et al. (2017), with the toe raised and translated onshore, encroaching into the dune. Dune slumping is handled by reclining the surface at the translated dune toe by the angle θ_{dune} (Fig. 6b), using a conservatively low angle for unconsolidated sediment of 30° by default (as per Kinsela et al., 2017), which can be modified. Note the dune is slumped from the base of the vertical 'sand cliff', as opposed to the mid-point as in Nielsen et al. (1992) and Kinsela et al. (2017), which allows buried cliff faces to become fully exposed, rather than being covered by slumped dunes. This is intended to replicate the observed behaviour at Perranporth and similar coastlines, where cliffs that experience greater erosion, and/or are more seaward, become fully exposed, by erosive wave action, and do not maintain an accumulation of slumped sediment in front of the cliff face. The slumping is implemented iteratively onshore from the dune toe after translation ($X_C(t_1)$), until the initial profile is intersected from below (Fig. 5b), which becomes the onshore point of closure (a)

$$z_i(x) = z_{i+1} + tan\theta_{dune}, a \le x_i < X_C(t_1) \tag{16}$$

As with all modifications to the profile, volume is conserved by determining the profile iteration distance (ΔX, Eq. 8) that minimises (Eq. 9).

3.4.3. Long-term trend sediment flux with the lower shoreface

A potentially important, though often neglected, budget component is gradual transport between the lower- and the upper shoreface (Dean and Houston, 2016; Anthony and Aagaard, 2020), occurring when a profile is out of equilibrium with forcing conditions (Cowell et al., 2001; Cowell et al., 2003; Daley and Cowell, 2012). If the lower shoreface bed lies above the ideal long-term equilibrium, sediment is brought onshore from the lower zone, which is inactive on short term scales (Cowell and Kinsela, 2018), forced by wave asymmetry to the upper zone, where material is regularly re-worked through cross-shore processes. Conversely, diffusive and gravitational processes (Stive and De Vriend, 1995), as well as mega-rips (Loureiro et al., 2012; McCarroll et al., 2016) may move material downslope to the lower shoreface. Reported rates of lower shoreface onshore transport are on the order of 1 to 5 m^3/m/yr (e.g., Dean and Houston, 2016; Kinsela et al., 2016), and it is hypothesised that similar rates may be common globally (Cowell et al., 2001).

In ShoreTrans, transport between the upper and lower shoreface is specified as a volume ($\Delta V_{x,\,L}$, Eq. 7). The point between the upper and lower shoreface (Z_{D1}) is held as a nodal point. Volume is removed or added from the lower shoreface as simple Sine half-wavelength, across the span from $W_L = X_{D2} - X_{D1}$ (Fig. 1). A Sine curve is chosen for simplicity and choice of shape does not impact the active shoreface, more realistic shape options could be added when data become available (Cowell and Kinsela, 2018; Anthony and Aagaard, 2020; Kinsela et al., 2020). The amplitude of the Sine curve is

$$A = \frac{\Delta V_{x,L}\,\pi}{2\,W_L} \tag{17}$$

And the change to elevation at each point on the lower shoreface is

$$z_i(t_1) = z_i(t_0) + Asin\left(\frac{[x_i - X_{D1}]\pi}{W_L}\right), X_{D1} < x_i \le X_{D2} \tag{18}$$

modifying the lower shoreface shape temporarily alters the total profile volume, which is restored by translating the active shoreface (Eqs. 8,9) to balance the change. An example of hypothetical onshore transport from the lower shoreface using Narrabeen, Australia, is shown in Fig. 7a.

The Narrabeen dataset (Turner et al., 2016; using profile P4, near the middle of the embayment) is used for demonstration as it is an indicative embayed beach setting for which detailed long term observational data (40+ years) are freely available. The examples in Fig. 7 are hypothetical in that they do not represent observed sediment transport processes. Z_{D1} and Z_{D2} in this case (Fig. 7) are set to −10 m and − 20 m respectively. Note the smoothing applied at the base of the active shoreface, in the case of a positive sediment budget (Fig. 7a), allows for some sediment to be transported below Z_{D1} (details in Section 3.1, '*Step-smoothing at the base of translation*').

3.5. Alongshore sediment fluxes and other sources / sinks

This section deals with sediment fluxes with the active profile that modify the total profile volume (ΔV_y and ΔV_{SS} in Eq. 7), resulting in non-zero values of ΔV in Eq. (9). Changes to total profile volume may occur due to a variety of processes, including: (i) longshore transport gradients; (ii) short-term beach rotation; (iii) headland bypassing; (iv) exchange between the shoreface and estuaries; and (v) dredging / nourishment activities. ShoreTrans simulates inputs and outputs to the profile budget by translating the profile on- or offshore, in the absence of SLR. This is the same method as applied in Fig. 3, with $\Delta S = 0$, i.e., the profile is not raised (skip step Fig. 3b) prior to translation.

An example of volume gain and loss is indicated (Fig. 7b), using Narrabeen (profile P4) as an example, showing a gain/loss of 250 m^3/m, hypothetically representing min/max rotation; however, it is noted that in reality, the primary mechanism of rotation at Narrabeen is alongshore variable rates of cross-shore flux (Harley et al., 2011). The maximum elevation for volume change can be applied at the dune toe or at the berm crest (by specifying different values of X_C, Z_C). This approach for estimating the rotation envelope will be used for Start Bay in Section 5.

3.5.1. Alongshore-balancing within embayments

The method shown in Fig. 7 is suitable for estimating long-term trends and short-term variability in longshore transport within an embayment, e.g., at Start Bay in the UK, where multi-decadal unidirectional flux is overlain by short-term oscillations (Wiggins et al., 2019; McCarroll et al., 2019a). However, for cross-shore dominated embayments, where rotation is insignificant, such as Perranporth (Valiente et al., 2019b), a different approach is required to account for alongshore sediment redistribution.

Considering a closed embayment backed by cliffs in some sections and dunes in others (Fig. 2a), dune erosion will be distributed unevenly across the bay. In this instance, the shoreline is assumed to be in equilibrium with the wave climate, and the eroded dune sediment, initially deposited in front of the dunes, will create a disequilibrium. Over time, alongshore processes are assumed to act to restore the initial shoreline alignment, evenly distributing the localised dune erosion across the entire alongshore extent of the bay. ShoreTrans accounts for this effect in a two-step process by calculating dune erosion separately for each profile, then combining this into a shared pool of total embayment dune erosion. For an individual profile (k), representing an alongshore length (L_k), the initial translation (without dune balancing) gives $\Delta V_{shoreface,\,k} + \Delta V_{dunes,\,k} = 0$ (as an interim step, volume is initially conserved within the profile), or alternatively $\Delta V_{shoreface,\,k} = -\Delta V_{dunes,\,k}$. The total dune erosion from this interim step is

$$\Delta V_{Dune,Total} = \sum \Delta V_k L_k \tag{19}$$

The second step divides total eroded dune volume evenly along the beach ($\Delta V_{shoreface,\,k} = -\Delta V_{Dune,\,Total}/L_k$), and the profile translation distance which balances the required volume change is determined (Eqs. 8,9). Volume is now conserved within the embayment, but individual profiles will change in volume. This method follows the move towards a 'compartments approach' where volume is conserved within an embayment (Kinsela et al., 2017, 2020).

3.6. Short-term cross-shore variability (storm erosion)

Variability in the cross-shore profile due to storm erosion of the beach and dunes is often the dominant short-term (1–10 year) component of shoreline variability on wave exposed beaches (e.g., Sallenger Jr, 2000; Masselink et al., 2016; Beuzen et al., 2019). Techniques exist for modifying a 2D-profile to simulate extreme erosion (e.g., Kriebel and Dean, 1993; Larson et al., 2004; Kinsela et al., 2017); however, these methods are generally profile-type specific and require a long-term record of historical observations to calibrate against. The development of a novel, generalised cross-shore variability model (i.e., storm erosion and recovery) is beyond the scope of the present work, but may be added in future. As a simple alternative, in our analysis of a cross-shore dominated embayment (Perranporth, Section 4), we opt for using long-term observations of change in shoreline position, then apply a conservative 3σ envelope (99.7% confidence interval, using the detrended shoreline position, assuming a normal distribution) to estimate maximum variability in shoreline position (not volume in this case), and assume the size of this envelope will remain constant over time (example using Narrabeen data, Fig. 7c). Other users may choose to apply the method of Kriebel and Dean (1993), or determine the envelope of shoreline position using satellite observations (e.g., Vos et al., 2019).

3.7. Probabilistic uncertainty and choice of inputs to model applications

Coastal management has seen an increasing move towards probabilistic, and away from deterministic, techniques to address uncertainty. We follow the approach of similar efforts (Cowell et al., 2006; Kinsela et al., 2017; Wainwright et al., 2015; Le Cozannet et al., 2016, 2019), using a probability density function (PDF) for key inputs to the model, e.g., depth limit of the upper shoreface (Z_{D1}) and sea level rise (Fig. 8). A normal or triangular PDF (Fig. 8) can be selected. A selection of random cases are sampled from the PDF and a translated profile is generated for each case ($n = 1000$ in Fig. 8). The resulting envelope of profiles can be used to visualise the potential range of shoreface change (Fig. 8c) and shoreline recession can then be viewed as a probabilistic histogram, with percentile likelihoods (Fig. 8d).

In order to assess a suitable sample size for model applications in Section 4 (Perranporth) and Section 5 (Start Bay), a preliminary test was performed on the Perranporth data set (using the range of inputs that will later be outlined in Section 4.1), comprising a single 'large' sample (n = 10,000), which was then split into 10 'small' sub-samples of n = 1000 for comparison. The test used to determine if there was significant variation between predicted recession rates (comparing between large and small samples), for the peak (mean) of the distribution and the 95'th percentile. Test results indicated minimal variation for the mean estimate of shoreline change (< 1 m) and marginally larger variations for the 95'th percentile (average difference between large and small samples of <1 m; maximum difference between samples of 3 m). This is deemed to be a sufficient level of convergence for demonstration purposes, and a sample of $n = 1000$ is used herein. However, a larger sample would likely be required in future applications to achieve convergence at the 99'th percentile (e.g.,Callaghan et al., 2008; Kinsela et al., 2017), or if a greater number of variables were to be modified.

A triangular distribution is used for all applications in Sections 4 and 5, which is applicable when there is some idea of a most likely value and the upper and lower bounds, but the exact shape of the distribution is poorly understood (Cowell et al., 2006). We use observations to inform model inputs where data exist, then use best estimates from the literature where no field data are available. The following applications are intended to demonstrate the capabilities of the toolbox, while also providing a first-pass (non-exhaustive) assessment of future shoreline change for the two sites (Section 2). More comprehensive future studies are required to address the finer details at each site, including coupling of ShoreTrans with a reduced complexity model (e.g., Vitousek et al., 2017a), to directly link the shoreface translation module to wave forcing, allowing for adaption to changes in boundary conditions (e.g., a change in wave climate) or dynamic feedback between the morphology and forcing (e.g., negative feedback as a rotating shoreline reaches equilibrium with the dominant wave direction).

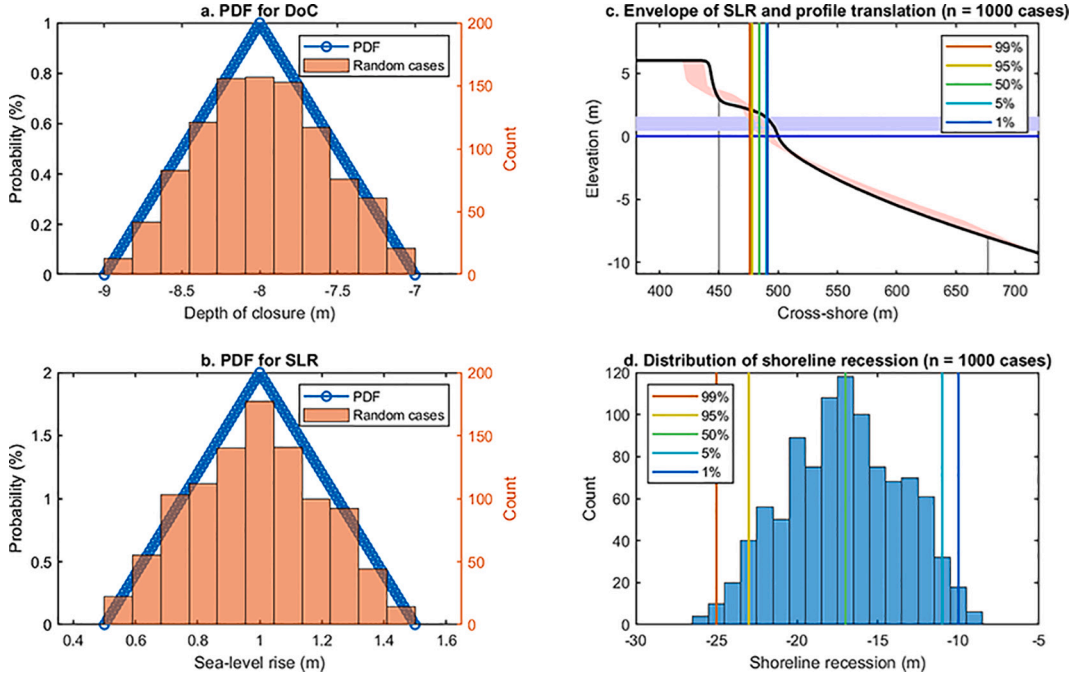

Fig. 8. Probabilistic treatment of uncertainty within ShoreTrans.

3.7.1. Sea level rise

We use SLR of 1-m over 100 years (i.e., from 2020 to 2120) for all scenarios, with uncertainty bounds of ±0.5 m for applications that include probabilistic uncertainty (Sections 4.2 and 5.2). This is approximately equivalent to extrapolating the IPCC high-emissions scenario RCP8.5, which estimates ~0.7 m of SLR by 2100, out to 2120. This approach provides a convenient benchmark for conceptualising SLR impacts (Section 6), while being within the bounds of real-world estimates. Other input variables are site-specific and are introduced within Section 4 and 5.

4. Results, Site 1: Perranporth

We now determine inputs and outputs to the Perranporth sediment budget and apply the ShoreTrans model to estimate future profile evolution. Beach-dune-bathymetric surveys extending back to 2007 (Fig. 2a-d, Fig. 9) were used as the primary data source. Morphological data were obtained using a multi-method approach, with extensive details given in (Valiente et al., 2019b). Profiles were extracted from a 2017 merged topo-bathymetry. A summary of model input parameters for Perranporth are given in Table 2.

The Perranporth intertidal undergoes annual 50–70 $m^3/m/yr$

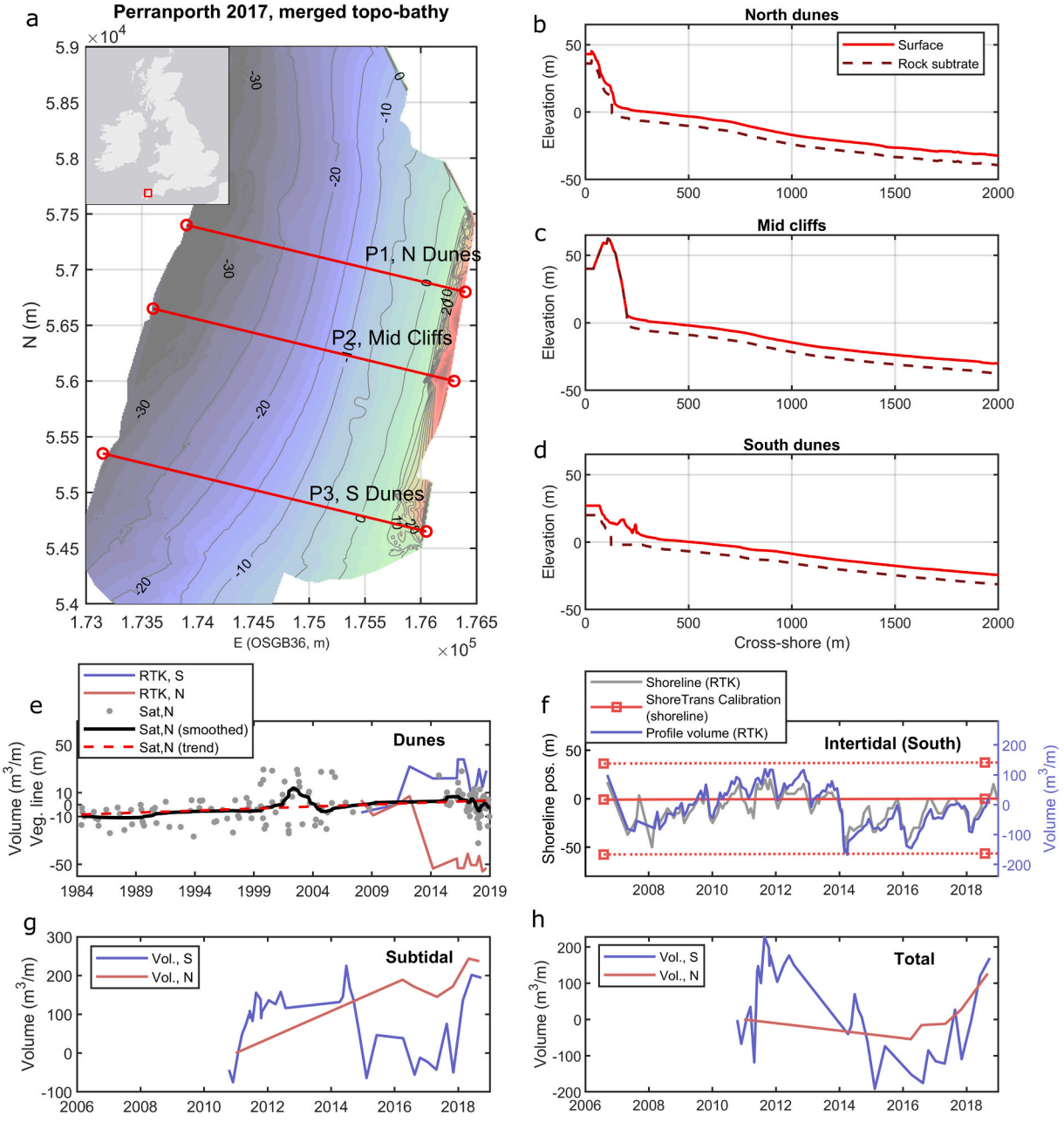

Fig. 9. Perranporth Beach with morphological change time series. (a) plan view of beach morphology, (b-d) three selected profiles; (e-h) volume time series for each component of the system (Dunes, Intertidal, Subtidal) and the Total cross-shore system, for the southern and northern sectors. For (e), 'RTK' is in units of volume alongshore, 'Sat' indicates the dune vegetation-line obtained from satellite imagery, with units of metres, the thick black line is a Robust Loess smoothing over 30% of the dataset, the dashed-red line is a linear trend. For (f), grey line is shoreline position (0 m ODN), with maximum storm erosion (Mar 2014) and time of full-embayment surveys (Aug 2017, used for a-d) indicated. For (h), solid red line is a ShoreTrans calibration of shoreline position from 2006 to 2030, with $\Delta S = 2$ mm/yr, red dotted lines estimate maximum shoreline variability using 3σ of the observed shoreline position (Fig. 6c). (For interpretation of the references to colour in this figure legend, the reader is referred to the web version of this article.)

Table 2
Perranporth model parameters.

Input parameter	Parameter details	Low bound*	Mean estimate*	High bound*	Comment
Elevations (m)					
Sea level rise (m)	ΔS, Eq. 8, Sec. 2.1	0.5	1.0	1.5	1 m over 100 years. Equivalent to extrapolating RCP8.5 to 2120.
Base of active profile	$-Z_{D1}$, Fig. 1 (Eq. 2–3**), Sec. 2	15	18.25	21.5	Low bound is observed DoC_1, high bound is $(DoC_1 + DoC_2)/2$, (Valiente et al., 2019a)**.
Base of profile change	$-Z_{D2}$, Fig. 1 (Eq. 3**), Sec. 2	–	28	–	DoC_2 from (Valiente et al., 2019a)**.
Inputs / Outputs					
Dune vertical aggradation (m^3/m/yr)	$\Delta V_{x,\,U}$, Eq. 7, Sec. 2	−0.25	0.25	0.75	Inputs / outputs represent first-pass estimates, based on observations (Valiente et al., 2019b) and modelling (Valiente et al., 2020), guided by an understanding of typical values (Dean and Houston, 2016; Cowell et al., 2001).
Longshore transport, as headland bypass (m^3/m/yr)	ΔV_y, Eq. 7, Sec. 2	−1	2	5	
Lower shoreface transport (m^3/m/yr)	$-\Delta V_{x,\,L}$, Eq. 7, Sec. 2.4	−1	2	5	
Cross-shore variability					
Max. obs. shoreline change (m)	Sec. 2.6	−47	0	47	Observed shoreline data, 3σ (99.7% conf. int.), offset to time of Aug 2017 survey (Fig. 9f).

* A triangular distribution (Section 3.7) was used to randomly select $n = 1000$ scenarios using the above parameter ranges for use in Section 4.2.
** Z_{D1}, Z_{D2} were determined here based on previous studies. In general, Eq. 2–3 can be used to estimate DoC_1 and DoC_2, and converted to values for Z_{D1}, Z_{D2} (see Section 2)

oscillations (Fig. 9f), and the upper shoreface to dune system exhibits large oscillations (± 200 m^3/m/yr) in total volume (Fig. 9h), attributed to headland bypassing as well as flux between the lower- and upper shoreface (Valiente et al., 2019b, 2020). The upper shoreface to dune systems appears to be dynamically stable to prograding, suggesting inputs to the system as high as +10 m^3/m/yr, but with large inter-annual fluctuations (Fig. 9h), and negative values for some multi-annual periods. As a supplementary line of evidence on long-term trend, the dune vegetation-line from satellite images has been examined, using a modified and unvalidated version of the CoastSat software package (Vos et al., 2019). Satellite images suggest the vegetation-line for the northern dunes has been relatively stable for the past 35 years (Fig. 9 'Dunes', black line), with 12 ± 6 m of progradation over this period, determined by fitting a linear trend to the unsmoothed average vegetation line (Fig. 9 'Dunes', grey dots), with 95% confidence intervals. This is also consistent with a stable to prograding system. The open nature of the Perranporth system (Fig. 9h) precludes an easy estimate of long-term (multi-decadal) trend rates, i.e., the noise due to natural short-term variability is much larger than the residual trend. We use the available data as a guide that the system may be prograding, though with large uncertainty, and make it clear that as future data become available, the understanding of the sediment budget in this embayment may change significantly.

Sea level rise is set to 1-m with ±0.5 m uncertainty (Table 2). For depth of closure, the annual observed depth of morphological change is DoC_1 = 15 m (Valiente et al., 2019a) relative to Ordnance Datum Newlyn (ODN, which is approx. Mean sea level), and the depth of no motion is DoC_2 = 28 m (both values from Valiente et al., 2019a). Model input for the base of the active profile (Z_{D1}) uses a triangular distribution with [lower; upper] bounds of $[-DoC_1;\ -(DoC_1 + DoC_2)/2]$, and a modal value as the midpoint between these, which equates to [15 m, 18.25 m, 21.5 m]. The base of sediment motion is $(Z_{D2} = -DoC_2 = -28\ m)$.

Inputs and outputs to the multi-decadal Perranporth sediment budget (Table 2, bottom half) are inferred from observations and modelling (Valiente et al., 2019a; Valiente et al., 2019b; Valiente et al., 2020). Based on this, and considering expected values from the literature (Cowell et al., 2001), a mean input of +4 m^3/m/yr and a range of −2 to +10 m^3/m/yr is used, distributed equally between headland bypassing (ΔV_y in Eq. 7) and cross-shore transport from the lower- to upper shoreface ($-\Delta V_{x,\,L}$ in Eq. 7), as these are unable to be differentiated (Valiente et al., 2019b; Valiente et al., 2020). In the absence of field data on dune aggradation ($\Delta V_{x,\,U}$ in Eq. 7), a range of −0.25 to 0.75 m^3/m/yr is applied, based on the literature (e.g., Stive, 2004), with the peak value (0.25 m^3/m/yr) equivalent to 5 mm annual vertical growth distributed over 50 m behind the foredune crest. The ShoreTrans tool was calibrated against the observed topographic survey record, running the model from the time of the full embayment survey (Aug 2017) for ±12 years, assuming a current rate of SLR of 2 mm/yr and using the sediment budget inputs/output as per Table 2 (solid red line in Fig. 8f). An estimate of short-term shoreline variability (±47 m) was obtained from variance of the observational record (Fig. 9f), taking a 3σ confidence interval and adjusting to account for the position of the Aug 2017 survey date shoreline within the total range (dotted red lines, Fig. 9f). This adjustment effectively accounts for the morphological state of the beach at the time of the full embayment shoreface survey. In this instance, the Aug 2017 shoreline lies at the 60th percentile (slightly more accreted than the long term average) and therefore the upper uncertainty bound (Fig. 9f), is smaller than the lower bound.

Profile selection is simplified by taking only three profiles along the extent of Perranporth (Fig. 9a-d). Each of the profiles represents a different backshore morphology type, including: (P1) Northern 'perched' dunes, overlying a shallow bedrock substrate, representing 50% of the total shoreline length; (P2) Mid-beach cliffs, 33% total length; and (P3) Southern dunes, with greater depth to bedrock and a shallower shoreface gradient, 17% total length. For P1, depth to bedrock is estimated at 7 m based on seismic surveys (work in preparation), with a horizontal distance from the foredune surface to the buried cliff face estimated as a minimum of 15 m, based on observations that >10 m of foredune retreat (Valiente et al., 2019b) failed to expose the cliff face for sections of the northern dunes. The buried cliff is set to behave as a wall once exposed (as per Section 3.2 and Fig. 4). The exposed cliff at P2 is set to act as a wall (Fig. 4a-c). Choosing fewer profiles is done for clarity in this brief example application; however, a detailed application could take many profiles at fixed intervals along the bay.

4.1. Perranporth: 100-year profile translation, with probabilistic uncertainty

The translation tool was applied to Perranporth using encroachment

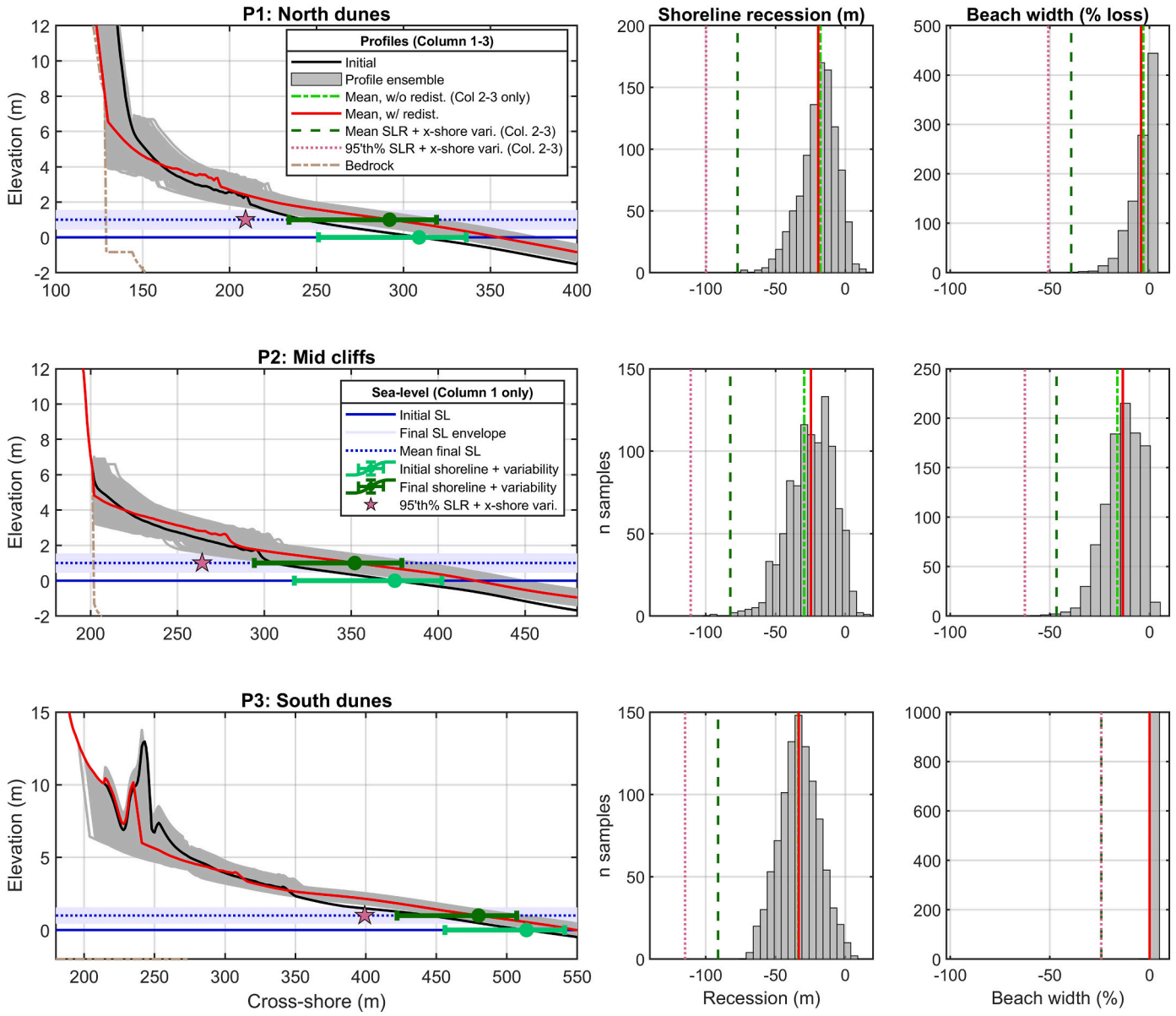

Fig. 10. PPT profile translation with projected shoreline recession and beach width reduction, for 1-m (± 0.5 m) sea-level rise over 100-years. (First column) Cross-sectional view of initial (black) and final (red) profiles, with profile ensemble envelope (grey), short-term cross-shore variability (green error bar) and rock layer (brown dash-dot). (Middle column) Shoreline recession histogram, with lines as per Col. 1, adding mean recession ignoring alongshore redistribution (light green) and 95'th percentile trend recession plus short-term variability (dark green dotted). (Third column) histogram of beach width percentage loss, with colour coding as per Col. 2. (For interpretation of the references to colour in this figure legend, the reader is referred to the web version of this article.)

mode (Section 3.3), given that the large dunes (10 m foredune height) and steep substrate gradient will act to prevent rollover from occurring. The results are given in Fig. 10. This application involves 1 time-step (2020 to 2120) with $n = 1000$ samples for each profile, randomly selected across the input ranges in Table 2, using triangular PDFs.

For P1, with 1-m SLR, the profile is predicted to recede to the buried cliff face (Fig. 10, top-left), where a maximum recession limit for the dune toe is reached. For higher rates of translation, the 'wall demand' increases ($\Delta V_{wall\ demand}$; Fig. 4) and the upper-beach profile flattens (spread of grey envelope in Fig. 10, top-left). For the exposed cliff face in P2 (Fig. 3, mid-left), $\Delta V_{wall\ demand}$ is also a factor and produces flattening of the profile at the cliff base. For all profiles, the range of cross-shore variability (dark green error bar) is greater than the envelope of trend change. For P3 (Fig. 10, bottom-left), an isolated foredune is present, which is eroded in some scenarios and preserved in others (grey envelope).

The shoreline recession histograms (Fig. 10, 2nd Col.) indicate significant variability alongshore. P1 shows the lowest mean recession (−19 m) as the dune initially acts as a buffer, providing sediment to the shoreface as it is eroded. P2 shows greater mean recession due to the absence of dunes. However, the middle profile also benefits the most once the eroded dune volume is redistributed evenly alongshore (Fig. 10 middle, red line; method described Section 3.4), with a reduction in predicted recession of 5 m (Fig. 10, middle; distance from green line to red line). The southern profile (P3) is predicted to have the highest mean recession rate, primarily due to the lower gradient of the shoreface. Change in predicted beach width also varies alongshore (Fig. 10, Col. 3) and is unrelated to shoreline recession. The perched-dune (P1) and cliff-backed (P2) profiles begin to lose beach width as the shoreline recedes while the dune-toe cannot translate onshore due to the hard-rock boundary. This results in moderate loss of beach width for mean trend rates (10% to 20%) with >60% reduction in beach width (Fig. 10,

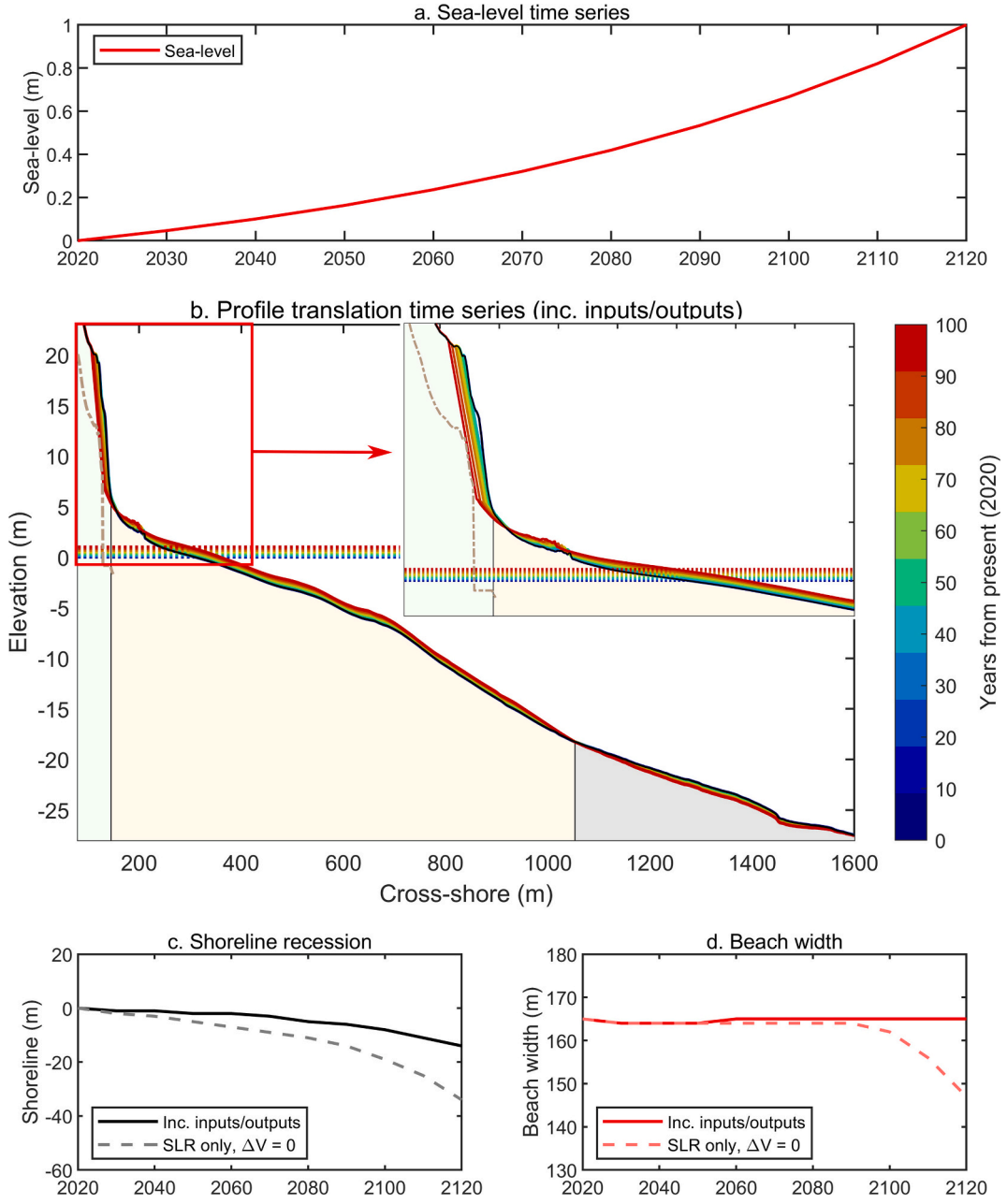

Fig. 11. Example profile translation time series for SLR of 1-m over 100-years, for profile P1 (North Dunes, Fig. 1), showing shoreline recession and beach width reduction. For (c), solid lines include inputs/outputs to the sediment budget and dashed lines are include SLR translation only.

second row, pink star to left and pink dotted line to right) at the extremes of cross-shore variability, i.e., after clusters of extreme storms. Note this width reduction is for a mean water level, and at spring high tide (6 m MSTR), the beach would likely be entirely submerged.

4.2. *Perranporth: time series for 1-m of SLR over 100-years*

We now apply the model to the northern Perranporth dunes (P1, Fig. 11) in an iterative time-series with 10-year increments (Fig. 11). For brevity and clarity, this application uses only the mean (peak probability) parameter values from Table 2, i.e., uncertainty ranges and cross-shore variability are not calculated. A hypothetical exponentially increasing sea level time series was calculated with length 100-years (Fig. 11a) to illustrate the time-dependent beach response.

In a scenario where sediment budget inputs are included, taking a combined input of 4 m^3/m/yr, split between headland bypassing (ΔV_y in Eq. 7; Table 2) and onshore flux from the lower shoreface ($-\Delta V_{x,\,L}$, in Eq. 7), it takes 100 years for the dune-toe to encroach back to the buried cliff face (Fig. 11b). During this time, there is a low rate of recession (~10 m by 2120; solid line Fig. 11c), while the beach width is stable (Fig. 11d). An alternate scenario for SLR translation only, with no sediment input (dashed lines Fig. 11c,d), indicates the dune toe would encroach back to the buried cliff face after 70 years, and beach width would begin to reduce after this time, highlighting the importance of including the non-erodible substrate. After 100 years, the SLR only scenario predicts greater than 30 m of recession and a 15 m reduction in beach width would occur. This suggests that positive sediment budgets may be critical in maintaining beach width for sites such as Perranporth, and highlights the need to better resolve inputs from the lower shoreface, which are currently highly uncertain (see Section 6.3). For clarity, note that the beach would periodically erode entirely to the buried cliff face well before the 70 to 100 years estimated in Fig. 11, with such

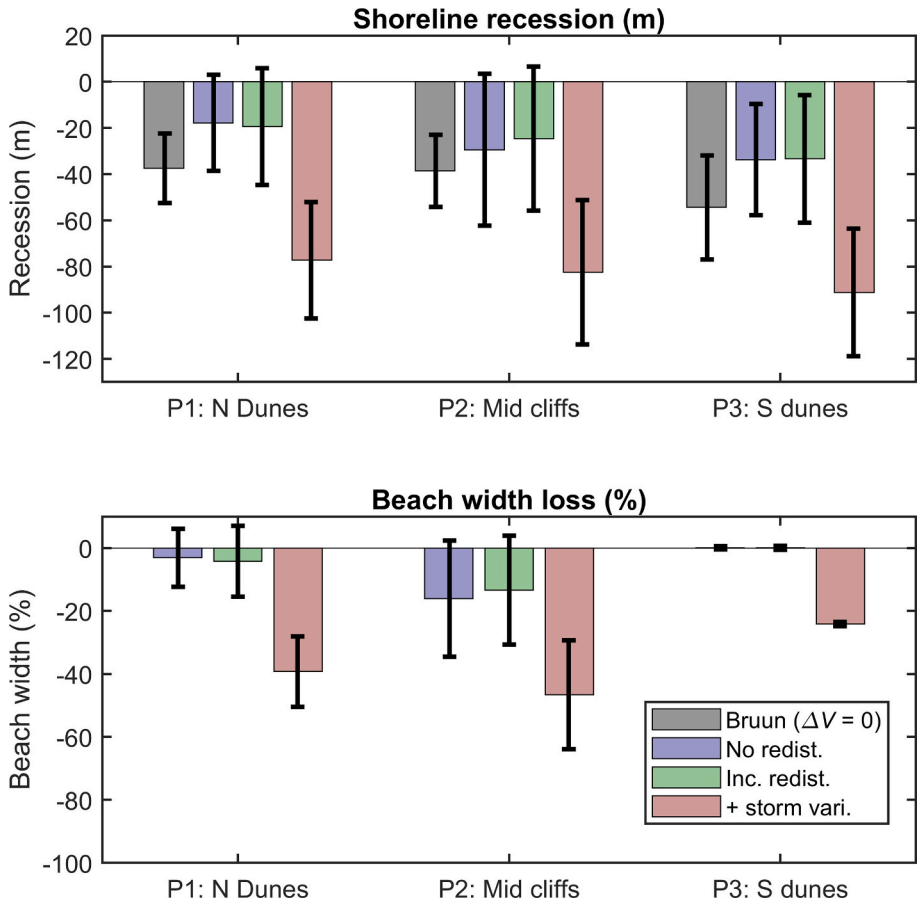

Fig. 12. Summary of shoreline recession and beach width prediction for Perranporth beach, assuming 1 +/− 0.5 m of SLR by 2120. The Bruun-rule is used for comparison of shoreline recession rates. Error bars indicate 1.96 standard deviations across the profile ensembles (as indicated in Fig. 9).

events occurring once the mean shoreline to cliff distance falls within the 47 m cross-shore variability range (Table 2). In addition, the large tidal range (MSTR = 6 m) would result in regular submersion of the beach as profile translation progresses. The joint-probability impacts of SLR, event scale variability and tidal range could be investigated using ShoreTrans to assess the future amenity of a given beach, though are not explored further here.

4.3. Perranporth: recession and beach width summary

A summary of predicted coastal change at Perranporth to 2120 is summarised in Fig. 12, comparing ShoreTrans against estimates using the standard Bruun rule (Eq. 2), without including other aspects of the sediment budget (cross- and longshore components in Eq. 7). Uncertainty is represented with 95'th percentile error bars (±1.96 standard deviations) of the ensemble sample (n = 1000; histograms in Fig. 11). Relative to the ShoreTrans tool, the Bruun Rule overpredicts shoreline recession (Fig. 12, top) as the positive sediment budget is not accounted for. However, in all instances, the error bars are overlapping, suggesting the Bruun rule is still an acceptable first-pass estimate for recession on this beach type. When cross-shore variability is added to the mean recession values (i.e., adding the maximum potential short-term storm erosion to the trend rate after 100-years), maximum recession distances are 2 to 4 times the base recession distance. Alongshore redistribution of dune erosion volume, where the sediment erosion from dunes is evenly distributed alongshore, is shown to be a minor factor in recession distances, but marginally offsets recession for the cliff-backed profile (P2).

The Bruun rule approach, and many recent efforts to predict future coastal change, focus on shoreline recession while neglecting beach width (Fig. 12, bottom). ShoreTrans estimates the greatest beach loss for the cliff-backed profile (P2, 10–20%), followed by the 'perched dunes and buried cliff' profile (P1), which lags due to buffering initially provided by the dunes (Fig. 11). The cliff-backed profiles show a greater beach width loss for extreme conditions, when cross-shore storm demand is added (>40% for P2), as the 'wall-demand' effect (Beuzen et al., 2018; Fig. 4) exacerbates storm impacts. By comparison, the southern dune profile (P3), which has no substrate exposure, is not predicted to lose beach width.

5. Results, Site 2: Start Bay

Morphological data for Start Bay were obtained using a multi-method approach, as described in (Wiggins et al., 2019). The profiles used herein were extracted from a 2018 merged topo-bathymetry (Wiggins et al., 2019). A longer record of shoreline change was obtained from tidally detrended satellite shoreline data (Vos et al., 2019), which shows trends consistent with the survey data (Fig. 13e). A summary of input parameters is provided in Table 3. SLR was projected at 1 ± 0.5 m by 2120, as for the Perranporth application (Section 4). Base of the active shoreface (Z_{D1}, Fig. 1) was obtained from observations around an extreme event (McCarroll et al., 2019a), taking the observed depth of morphological change as the shallow bound, with a range of 2 m, increasing from south (<10 m depth) to north (up to 12 m depth). An assumption of zero-transport is applied between the upper- and lower shoreface, due to the observed gravel-sand transition. Therefore, no lower depth of closure is specified, as no change to the lower shoreface will be applied within the model.

Inputs and outputs to the Start Bay application are applied as a gross rate based on the observed rates of shoreline change, with an assumption that 100% of volume change is attributable to longshore flux gradients,

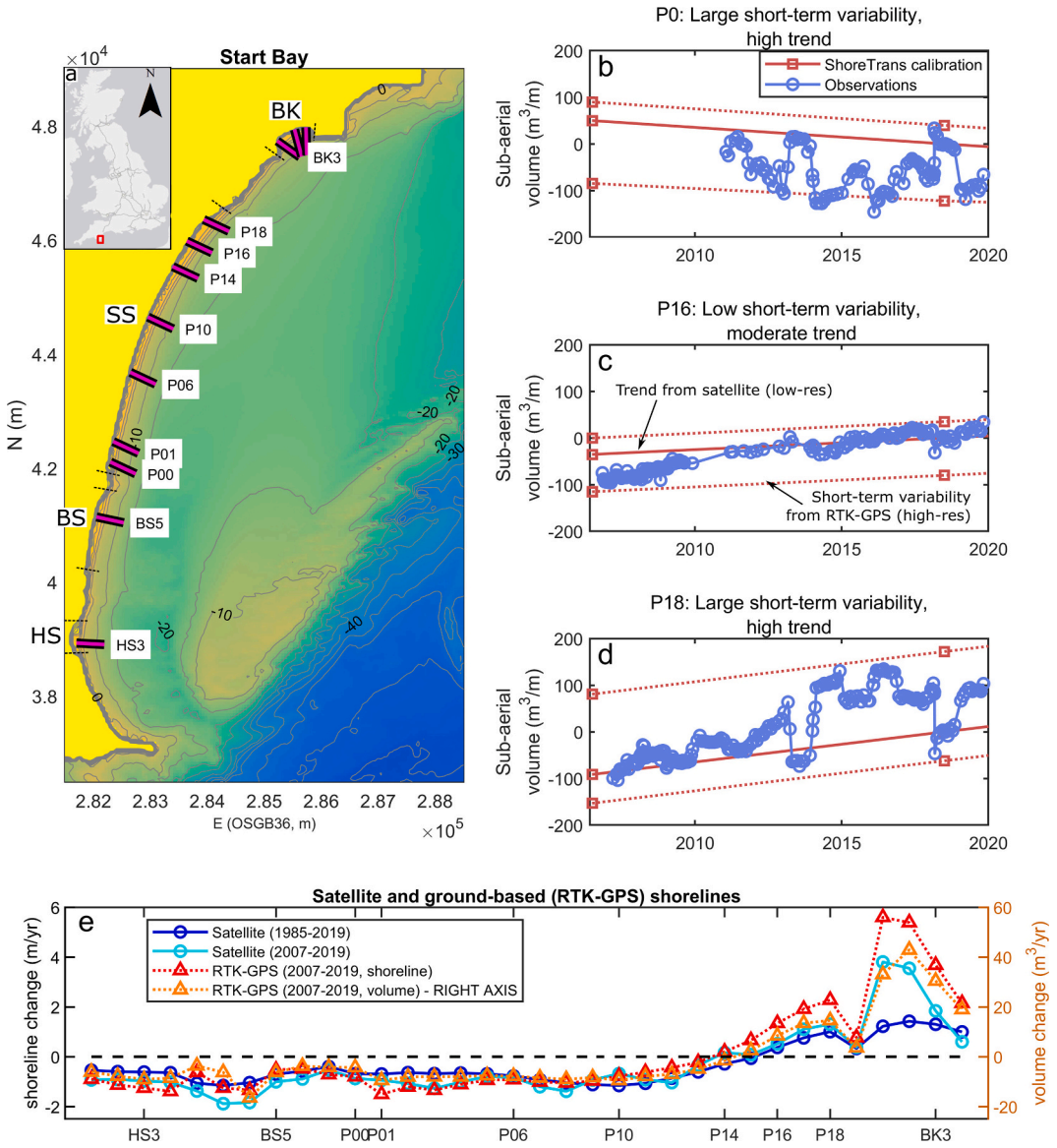

Fig. 13. Start Bay morphology and morphologic change. (a) Plan view with profiles indicated, beach names are Hallsands (HS), Beesands (BS), Slapton Sands (SS) and Blackpool Sands (BS); (b-d) Selected profile volume time series', illustrating differing behaviours in trend and variability; and (e) alongshore profile position against rates of shoreline change, comparing rates derived from satellite imagery and ground-based surveys.

which is considered a reasonable first-pass assessment for this setting (McCarroll et al., 2019b). The process is as follows: (i) trend changes to shoreline position were determined as a rate (m/yr) based on the long-term (1985–2020) satellite derived rate [Fig. 13e]; (ii) uncertainty bounds of ±0.3 m/yr were applied, rounding up the linear regression 95% confidence interval on the annual shoreline trend, using un-smoothed satellite based shoreline positions [maximum uncertainty is 0.24 m/yr, rounding up to 0.3 m/yr]; (iii) the translation model was initially run with zero SLR to determine the rate of volume change that equates to a given rate of shoreline change for each profile, thereby accounting for volume change across the entire active shoreface; (iv) a calibration was performed by projecting the trend sub-aerial [> -2 m ODN] volume changes [based on satellite data] from the survey date [July 2018] ±12 years, with the envelope of short-term variability determined as the range covered by the high-resolution RTK-GPS observations, rounding up to the nearest 10 m^3/m. Short-term variability is generally highest near headlands. Fig. 13b-d visually summarises the outputs of this extended process for three example profiles. For the wall-backed profile P0, (Fig. 13b), some observation points lie marginally below the variability envelope due to complexities of erosion occurring behind the sheet-piling, which are not covered in the simulation.

This approach assumes: (i) recent trend rates of volume change are likely to continue until 2120; (ii) sufficient sediment volumes are present at the southern end of the bay for the trend to be maintained; and (iii) the barrier will be stationary in the absence of SLR or longshore flux gradients. The validity of these assumption will be discussed in Section 6. The 'wall demand' method (Section 3.2) is applied to the sheet piling wall for the profile at Torcross (P0, Fig. 14a). For all other sections of the barrier, both the 'dune rollover and keep-up' (Type 2) and the 'encroach' (Type 4) methods were tested (Section 3.3, Fig. 5). The 'barrier rollover' method (Type 1) was not included as the lagoon-side barrier toe is not surveyed and Type 2 will produce similar results for large translation distances (e.g., Fig. 14, P1). Implicit in this approach is an assumption that the section of barrier that is currently crested by an asphalt road (P1 to P14, Fig. 13) will be permitted to naturally roll back.

Table 3
Start Bay model parameters.

Input parameter*	Low bound	Mean estimate	High bound	Comment
Elevations (m)				
Sea level rise (m), ΔS, Eq. 8.	0.5	1.0	1.5	
Base of active profile ($-Z_{D1}$, Fig. 1) … at **south** end of bay (m)	9	10	11	Low bound from observation (McCarroll et al., 2018), high bound inferred from depth of gravel barrier).
… at **north** end of bay (m)	10	11	12	
Profile trend rates of change (m/yr)		**Mean trend (±0.3 m/yr)**		**Short term variability (rotation) (± m^3/m)**
HS3 (Hallsands)		−0.6		−170/+150
BS5 (Beesands)		−0.7		−60/+150
P0 (Torcross, South Slapton Sands)		−0.7		−300/+90
P1		−0.7		−240/+90
P6		−0.8		−60/+100
P10		−1.2		−210/+150
P14		−0.3		−140/+80
P16		0.4		−170/+80
P18 (North Slapton Sands)		1.0		−130/+360
BK1 (West Blackpool Sands)		1.2		−1200/+150
BK3		1.3		−500/+210
BK4(East Blackpool Sands)		1.0		−420/+470

* A triangular distribution (Section 3.7) was used to randomly select n = 1000 scenarios using the above parameter ranges for use in Section 4.2. Methods to obtain mean trend and variability are described in the text.

5.1. Start Bay: 100-year profile translation, with probabilistic uncertainty

A wide range of profile translation responses are predicted across Start Bay. Three examples are selected: (i) a wall-backed profile, exposed to high rates of short-term variability and potential long-term extinction [Fig. 14, top]; (ii) a narrow receding section of the lagoon-backed barrier [Fig. 14, middle]; and (iii) a wide section of the barrier that is predicted to prograde in the future.

The first profile (P0, Fig. 14, top) is protected by cemented rip-rap on the upper profile, bounded below by sheet-piling (solid vertical black line). The initial P0 profile has a large range of natural variability (Fig. 14, top, grey dashed bars), due to alongshore rotation processes, and the location of the profile adjacent to a headland. Under the mean trend scenario, this profile is predicted to erode severely to below the raised sea level, with the toe reaching the MLWS limit of −2 m. The toe of the beach remains marginally above sea level when trend rates of shoreline change are ignored (green line). As the profile is depleted back to the wall (or near to it) for all scenarios, both short-term variability and shoreline recession converge on a single value (Fig. 14, top-right). The progressive erosion of this profile is explored further in Section 5.3.

The second profile (P1, Fig. 14, middle-row) includes various scenarios for a low-barrier, backed by a lagoon. Here, SLR translation is secondary to the trend rate of change (compare the green and red lines). Comparing the 'encroachment' and 'rollover and keep-up' scenarios (yellow and red lines respectively), encroachment results in 10 m less shoreline recession. However, this effect is dwarfed by the total amount of recession (~110 m) and also by the range of uncertainty in the ensemble (± 40 m). The third profile (P18, Fig. 14, bottom) is predicted to have a SLR recession impact of −20 m, which is overwhelmed by the long-term positive longshore budget and progradation trend. Despite the large range of natural variability (+360 m^3 for P18, Table 3), the range of uncertainty due to the trend change is larger still (pink dashed and dotted lines fall well within the shaded envelope / histogram). Beach width gain/loss for these cases are: −100% for P0 (for the mean trend), 0% change for P1 where the barrier is assumed to translate onshore and maintain width, and more than +50% for P18 which is prograding and is backed by a cliff.

5.2. Start Bay: 100-yr time series

ShoreTrans is now applied in time-series mode to the heavily defended profile P0, with 1-m SLR (Fig. 15) for the satellite-derived trend shoreline rate of −0.7 m/yr (Fig. 15, left column) and for zero trend, conserving volume (Fig. 15, right column). When the trend volume is included in the translation (Fig. 15, left column), the already narrow beach begins shrinking rapidly, mirroring the rate of shoreline recession (Fig. 15b-c). After 30-years of trend erosion, the bed level at the base of the wall passes below mean sea level (Fig. 15b,c). At this stage, the large variability due to rotation would result in an ephemeral beach, reappearing when easterly events force southward transport. After 50 years (Fig. 15c), the bed at the toe of the wall erodes to −2 m ODN and the beach is predicted to be extinct. By contrast, when only SLR is applied (zero trend, Fig. 15d-f), the beach width is more gradually depleted, with the remaining beach width at 10 m at the end of the 100-year period (Fig. 15f).

5.3. Start Bay sediment budget and shoreline recession summary

A present-day sediment budget was predicted for Start Bay (Fig. 16, top). The budget was calculated by first using the translation model to determine annual rates of volume change, based on the input rates of shoreline change in Table 3. Error bars are ±0.3 m/yr on the long-term trend (not including short-term variability). Volume change at each profile was multiplied by the distance alongshore represented by each profile. To maintain simplicity and brevity, the uncertainty introduced by using widely spaced profiles to represent alongshore variable morphology was not accounted for in this instance (see McCarroll et al., 2019a for a more detailed approach). Flux rates (Q; m^3/yr) are the alongshore integral of the volume changes at each profile, with positive values indicating northward transport. The budget indicates a northward flux, peaking within a range of 50,000 to 120,000 m^3/yr at P14. Despite the simplicity of this approach, the predicted flux rate approaches zero at either end of the embayment (within uncertainty bounds), consistent with the understanding that the Start Bay longshore sediment budget is closed to north and south (Wiggins et al., 2019). This implies that the current rate of shoreline translation in Start Bay (with negligible sea level rise) may be primarily attributed to longshore transport fluxes, with limited overwash and rollback potentially offsetting some of the residual positive flux.

The second panel of Fig. 16 displays a comparison of the SLR-only (no trend) forced shoreline recession predicted by ShoreTrans, against predictions using the Bruun rule. Here, recession rates are generally 10–30% greater along most of the bay. This is due to rollover of the barrier, which requires onshore transport, thereby increasing recession rates (Eq. 6; Rosati et al., 2013). This effect is greatest (>30% increase in recession) where the barrier is narrow and the back-barrier drops down to a lagoon (e.g., P01, P10). Comparatively, onshore transport is reduced where the barrier backs on to a cliff (e.g., P18) and the model predicted shoreline recession will approach the Bruun-predicted rate.

6. Discussion

6.1. Summary of site applications

The outcomes of the application of ShoreTrans to Perranporth

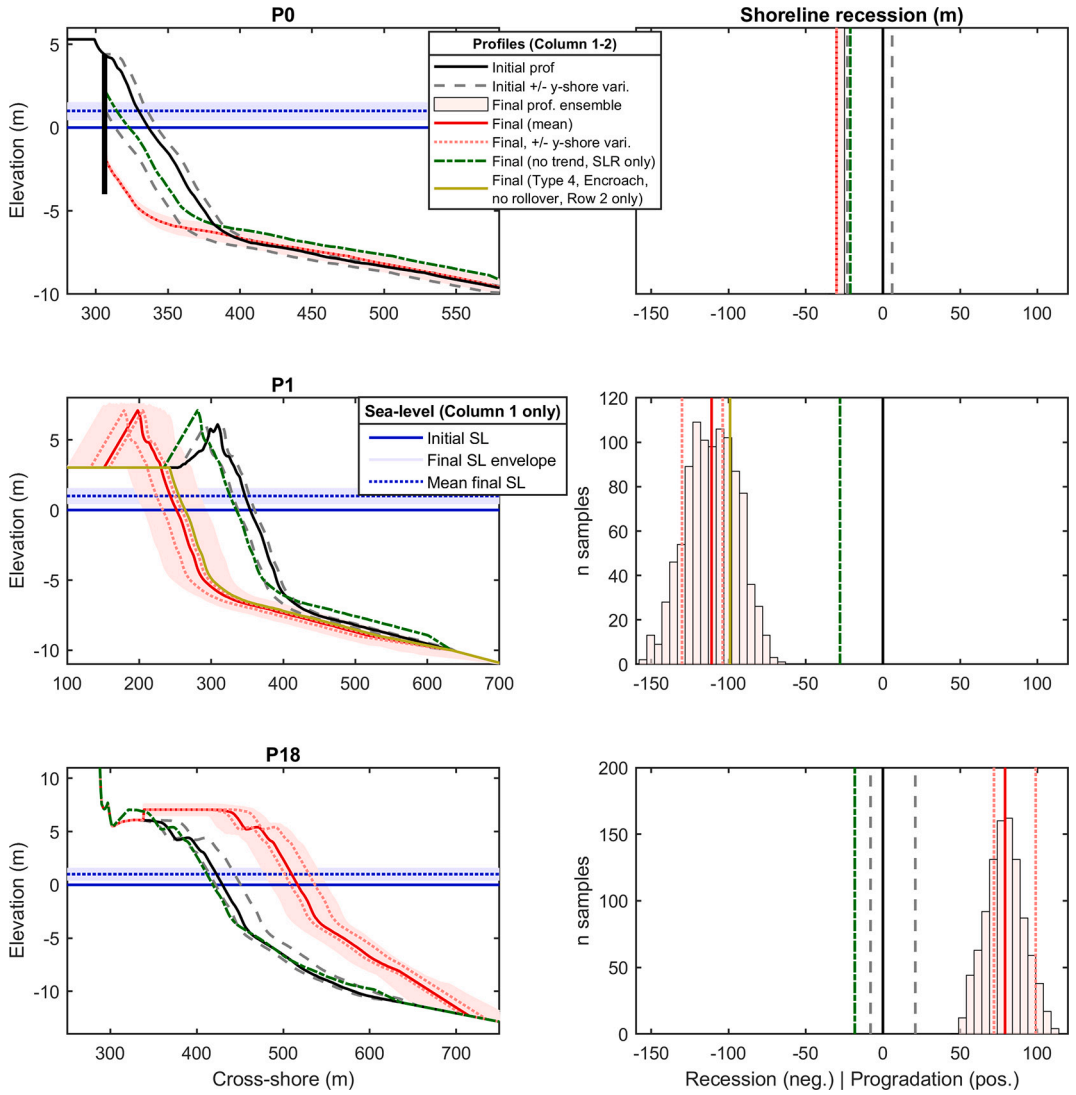

Fig. 14. Start Bay profile translation for three selected profiles with projected shoreline recession and beach width reduction, for 1-m (± 0.5 m) SLR over 100-years. (First column) Cross-sectional view of initial (black) and final (red) profiles, pre-SLR alongshore variability (grey dashed), with post-SLR profile ensemble envelope (pale pink), post-SLR short-term alongshore variability (pink dotted) and post-SLR profile, ignoring trend (green). (Right column) Shoreline recession histogram, with line colour and style as per Col. 1. (For interpretation of the references to colour in this figure legend, the reader is referred to the web version of this article.)

(Section 4) and Start Bay (Section 5) are summarised in Table 4, comparing the sites by the factors that contribute to short and long-term variations in shoreline position. The primary forcing controls on shoreline position at Perranporth are cross-shore variability and SLR, both contributing up to 50 m to shoreline change. Long-term trends at Perranporth (bypassing and transport with the lower shoreface) are also potentially critical, but there is large uncertainty around these values. By contrast, for Start Bay the dominant effect is the long-term trend in longshore flux towards the north of the bay. Note that we have assumed the trend from 1985 to 2020 will continue for the next 100 years, which may not be the case if long-term climatic variations impact on wave direction (Scott et al., 2021). For Start Bay, SLR is a secondary factor, contributing less than a third to the recession forced by the long-term trend in longshore sediment flux. Short-term alongshore variability at Start Bay is an important secondary factor, but only near headlands (Fig. 14, top). Additionally, it is noted that short-term cross-shore storm erosion was not modelled at Start Bay; however, this process may be of secondary importance for some profiles (de Alegria-Arzaburu and Masselink, 2010; McCarroll et al., 2019a; McCarroll et al., 2019b).

There is a high degree of variability both between and within sites, demonstrating the importance of applying a site-specific model that can adapt to complex geomorphic setting, such as ShoreTrans, when predicting shoreface evolution. Both the application sites are macrotidal and not necessarily indicative of other beach types; therefore, a future application to microtidal beaches (e.g., Narrabeen, Australia; Turner et al., 2016) would be of benefit.

6.2. A conceptual approach to shoreface change

We now expand from site-specific applications to a generalised, idealised, conceptual model (Fig. 17), demonstrating how ShoreTrans can be applied to demonstrate previously described relationships between profile geometry, barrier response mode and shoreline change (Roy et al., 1994; Cowell et al., 2003, b; Cowell et al., 2006; Wolinsky and Murray, 2009; Moore et al., 2010; Cowell and Kinsela, 2018; Anthony and Aagaard, 2020). This approach allows for a broader understanding of how shoreface change is sensitive to SLR and other input variables, which will facilitate further contextualisation of our results with the literature.

A reference case is selected (Fig. 17-top, #4 'Small dune, encroach'), using a power-law profile (Dean, 1977; $z = Ax^m$; where z is bed elevation and $A = 0.25$, $m = 0.67$), with a 50-m wide berm, a 6-m high dune crest,

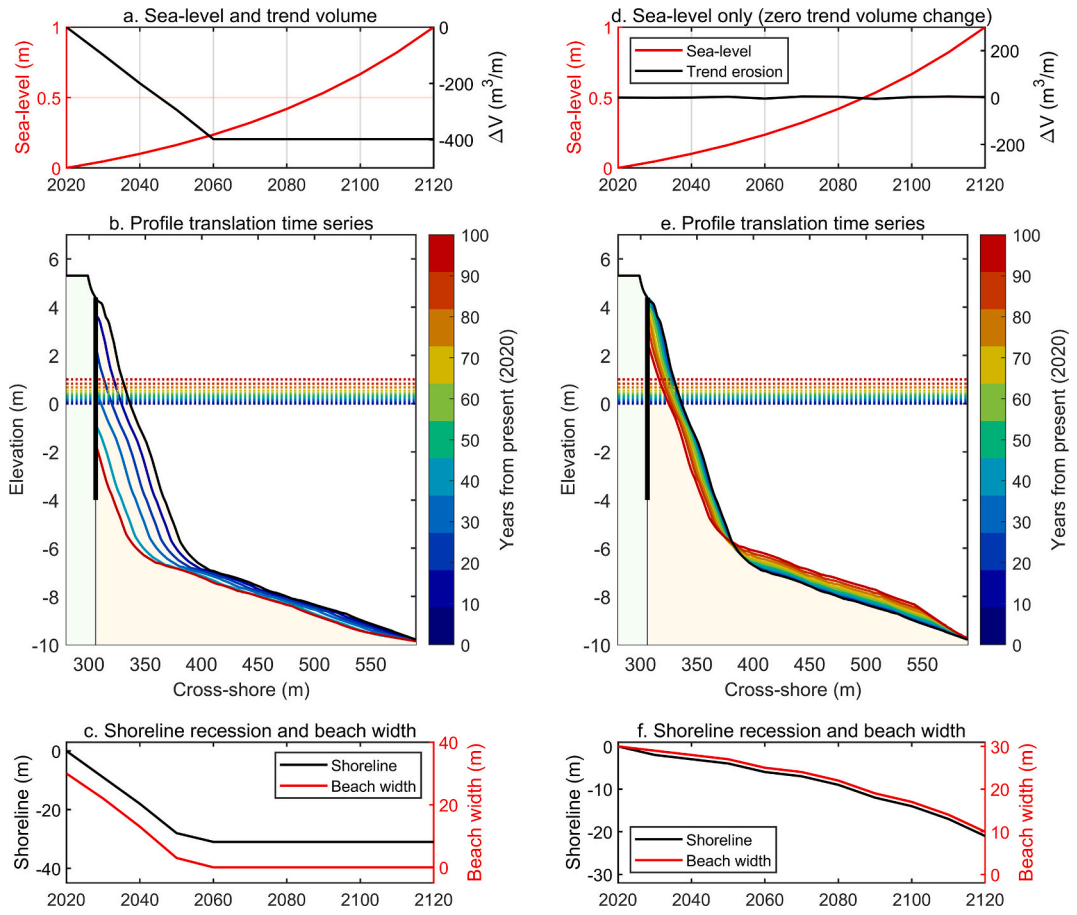

Fig. 15. Example profile translation time series for 1-m SLR over 100-years, with trend volume change included (−0.7 m/yr, left column) and zero trend change (right column), showing shoreline recession and beach 'extinction'. This is a heavily defended profile at Torcross (P0, Fig. 14), where sheet-piling (vertical bold black line in b and e) fronts cemented rock armour, backed by a promenade.

and the dune toe at $z = 3$ m. Shoreline recession is compared against a range of profile shapes (varying barrier/dune height, shoreface slope) and translation types (full rollover to encroachment). For all scenarios, a single representative SLR scenario of 1-m over 100-years is simulated, which is approximately equivalent to extrapolating the IPCC high-emissions scenario RCP8.5 to 2120.

Varying translation type (Fig. 17-top, vertical axis) leads to recession rates being maximised for 'full rollover' (3 times the reference case), where the barrier translates onshore through overwash using the lagoon-side barrier toe as the translation point (Fig. 17, Profile #1). Here, sediment flux is directed exclusively onshore (red line in bottom sub-panels shows onshore-offshore flux rates), consistent with the generalised Bruun rule (Eq. 6). Recession rates are reduced if 'encroachment' is assumed (Fig. 17-top, horizontal axis), with all sediment flux directed offshore, as per the standard Bruun rule (Eq. 5). Increasing dune height (Fig. 17-top, #8) results in additional supply for offshore transport for every horizontal metre of dune erosion, and therefore reduces recession in encroachment mode. Similarly, a steeper shoreface on a concave-up profile (Fig. 17-top, #9; $A = 0.3$ in $z = Ax^m$) reduces the new accommodation space generated for each incremental increase in sea level, also reducing recession.

For the reference case profile (Fig. 17), with an active profile width of W_a= 300 m, sediment inputs on the order 3 m^3/m/yr are sufficient to counteract the predicted impact of SLR (Fig. 18, top row). The inputs in this instance can be any cross- or longshore inputs to the active profile, including longshore transport gradients, onshore transport from lower shoreface, headland bypassing, nourishment, or estuarine exchange, derived using the methods in Section 4.1 and 5.1, or other similar approaches.

Calculation of sediment input required to offset SLR for an idealised profile is straightforward, taking (Eq. 7) and combining all sources of sediment input to the active profile (all ΔV terms), substituting zero for ΔX and taking the standard Bruun rule (Eq. 5) as the SLR function, the rate of ΔV required to offset SLR is

$$\Delta V_{offset}\left(\mathrm{m}^3/\mathrm{m}/\mathrm{yr}\right) = \frac{\Delta S}{\Delta t} W_a \tag{20}$$

Assuming a rate of SLR of $\Delta S/\Delta t$ = 0.01 m/yr and Bruun-type translation (encroachment), a wide dissipative shoreface like Perranporth ($W_a \approx 1000\ m$) requires O(10 m^3/m/yr) to offset SLR translation effects, while a steeper shoreface like Start Bay (or the reference case in Fig. 17; $W_a \approx 300\ m$) requires O(3 m^3/m/yr) to offset SLR effects. For real-world profiles, the net change in volume must also account for onshore transport from the active profile (Stive, 2004) to the dune ('encroachment mode', Table 1, Type 4; plus 'dune accretion', Eq. 15) or back barrier ('rollover' mode, Table 1, Types 1–3).

The value of ΔV_{offset} represents a key concern for coastal managers globally, who are seeking to maintain beach width under rising sea levels. For any wave-dominated shoreline, it is necessary to narrow the uncertainty bands on sediment fluxes to the system, which for both sites in this study may be as large or greater than the magnitude of SLR translation, but are of particular importance for wider active shorefaces (e.g., for Perranporth, Fig. 11c). Any deficit in ΔV_{offset} then becomes the target for future beach nourishment (e.g., Erikson et al., 2017).

Beach width changes are shown to be a function of wall/cliff position (Fig. 18, bottom row), when other inputs are fixed, taking the initial beach width as the distance from the wall to the shoreline, before SLR.

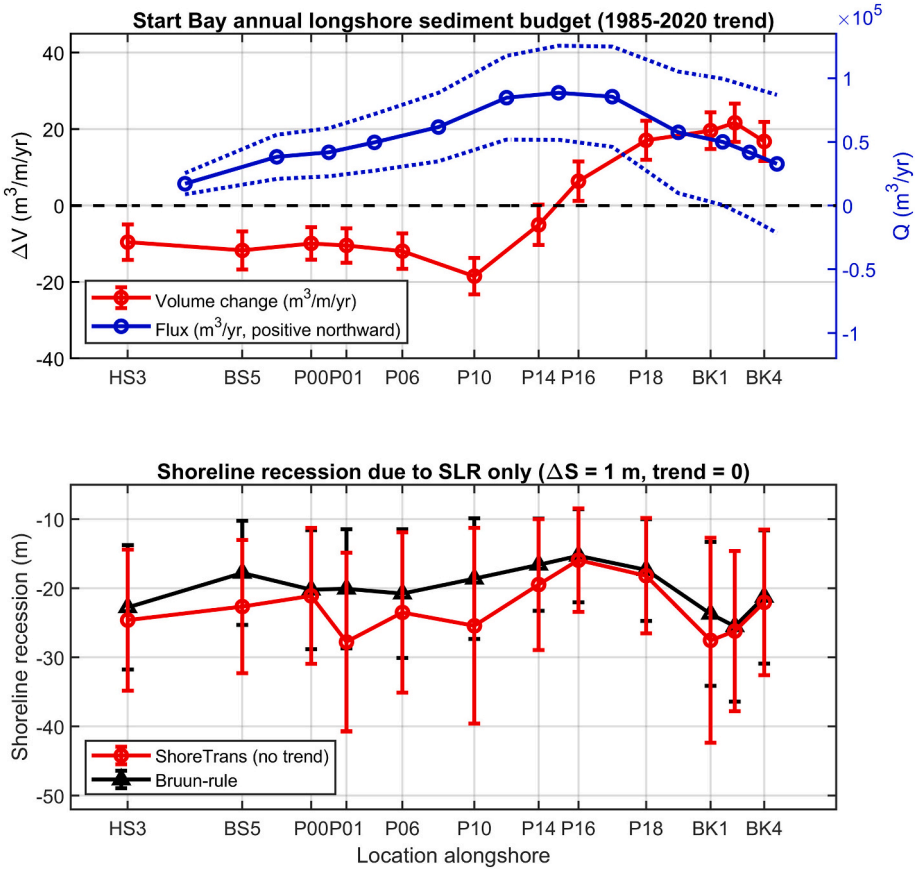

Fig. 16. STB full bay sediment budget. (Top) Translation model predicted volume changes over the period 1985–2020. (Bottom) Translation model predicted recession for the SLR component, compared against Bruun-rule estimate.

Table 4
Summary of predicted shoreline impacts for Perranporth and Start Bay of 1-m SLR over 100-years, comparing long-term trend and short-term variability.

Time-scale	Process	Perranporth	Start Bay
Long-term (multi-decadal)	SLR	**Primary (−30 to − 50 m recession)**	**Secondary (20 to 30 m recession)**
	Trend inputs/outputs to active profile	**Primary (potentially), with high uncertainty (−10 to + 40 m to shoreline position)**	**Primary (>100 m shoreline recession at south and progradation to north)**
Short-term variability (event scale to < 10 years)	Cross-shore (storm erosion)	**Primary (up to 50 m shoreline variation)**	*(Not examined, may be important for some profiles)*
	Longshore (rotation)	*(Not examined, assumed minor)*	**Secondary near headlands (±30 m).** **Minor at centre of bays.**

The relative contribution of processes impacting shoreline position are classed as primary (red), secondary (orange) and minor (green).

For the given idealised profile and SLR scenario, a buried wall or cliff located at the initial dune crest will force a beach width reduction of 20%. A wall at the dune toe will result in a 50% beach reduction, while a wall placed at the berm crest will cause the beach to be entirely eroded. While it is intuitive that a narrower initial beach will result in greater width loss for a given sediment volume demand, the ShoreTrans model explicitly addresses the additional wall-demand volume (Section 3.2) and quantitatively estimates the reduction in beach width for a given wall position. Shoreline recession is also impacted by the presence of a seawall (not shown); however, the result is non-linear and can be misleading. For example, a more seaward wall will exacerbate shoreline recession due to the 'wall-demand' effect (Beuzen et al., 2018) but if the wall is sufficiently far offshore, the beach will be lost entirely, while the wall ensures the shoreline remains fixed (cf., Figs. 12, 16).

6.3. Limitations and future development

6.3.1. Validation

ShoreTrans is presented here as an exploratory instrument, used for investigating hypotheses related to profile translation and sediment budget uncertainty. The tool has been calibrated to the two analysed sites (Fig. 9f, 12b-d), but the rules themselves rely on validation by pre-existing studies, and the degree of validation of different components varies. The tool is modular, and has been designed to assess the two test sites (Perranporth and Start Bay); however, additional rules can be added for future applications.

Regarding sea level rise translation, the combined use of the Bruun rule while also, critically, accounting for other aspects of sediment budget, have been validated in part (e.g., Zhang et al., 2004; Dean and Houston, 2016), and are supported by geological evidence (e.g., Fruergaard et al., 2015, 2021; Kinsela et al., 2016), but will rely on higher

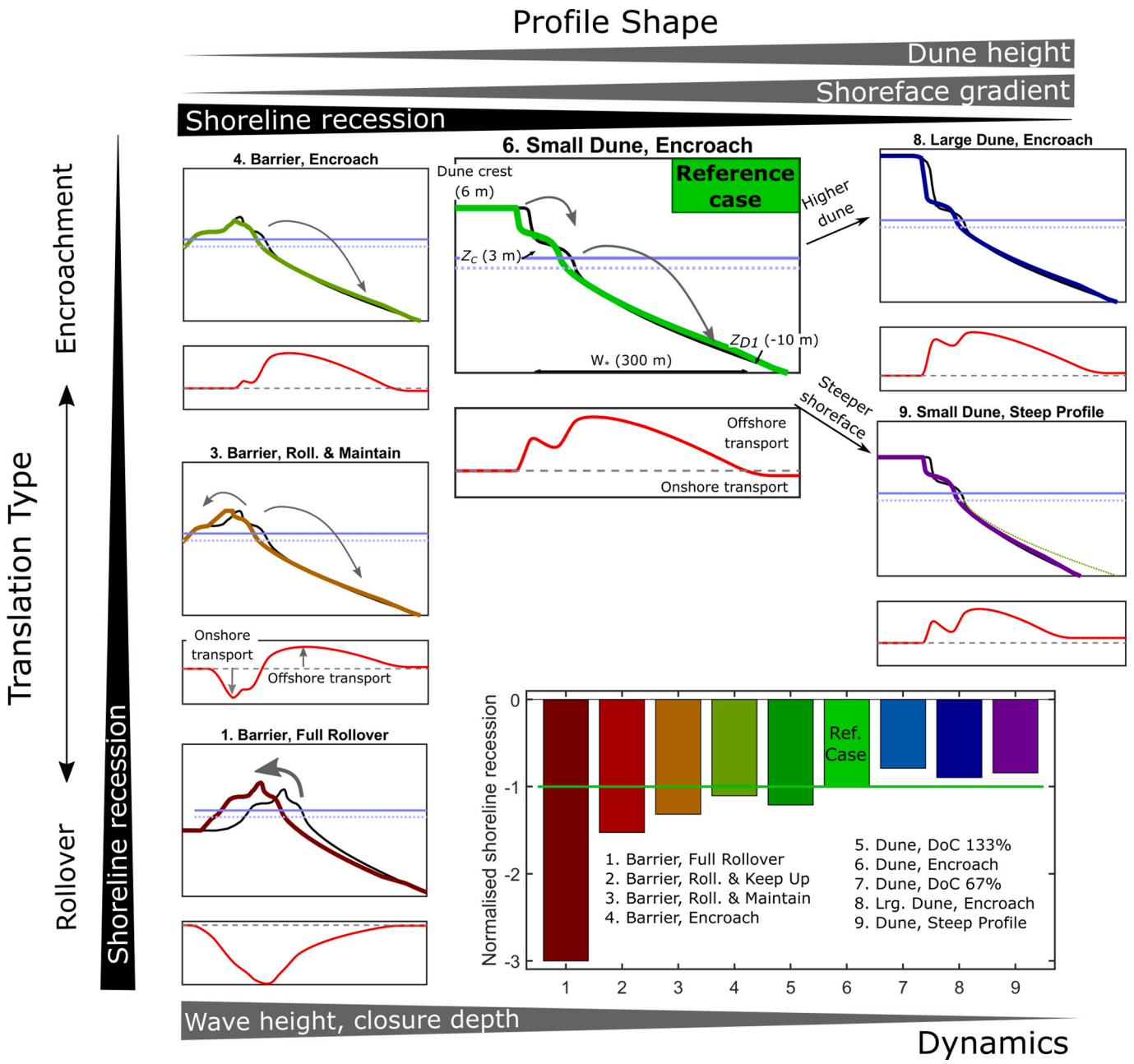

Fig. 17. Conceptual model of profile translation. A simulation of 1-m SLR over 100-years has been applied to all profiles, displaying recession rates for a range of translation types and profile shapes. The reference profile (#6) is based on a power-law profile below MSL ($A = 0.25$, $m = 0.67$), with a 50 m wide berm, upper depth of closure at z = −10, dune toe at z = 3 and dune crest at z = 6. For each displayed profile, the top sub-panel shows the initial and final profile, the bottom sub-panel (red line) indicates relative rates of onshore-offshore sediment flux. Profile #5 and #7 on the upper bar plot represent increases or decreases in depth of closure. Arrows indicate direction of sediment transport. (For interpretation of the references to colour in this figure legend, the reader is referred to the web version of this article.)

rates of future SLR for more precise validation. The degree to which a given profile will 'rollover' or 'encroach' is highly uncertain for low barriers (e.g., Rosati et al., 2013), while for dune-backed profiles where overwash never occurs, encroachment can be safely assumed. Another aspect of the toolbox that requires field validation is the 'wall-demand' effect, where erosion for a wall-backed profile is concentrated in front of the wall, which has only been quantified in a laboratory setting (Beuzen et al., 2018).

One of the most uncertain aspects of how shorefaces will translate is the response of the lower shoreface and defining the base of the active shoreface (Cowell and Kinsela, 2018; Anthony and Aagaard, 2020). Past rates of transport have been calibrated by retroactive fitting to a prograding site (e.g., Kinsela et al., 2016), but validation of translation models of lower shoreface flux (e.g., Thom et al., 1981; Daley and Cowell, 2012) are extremely difficult given the slow rates of change at these depths, relatively to the uncertainty of observational methods. The simplistic Sine-curve shape of modification of the lower shoreface used here (Fig. 7a) is intended only for volume conservation and may not reflect the expected decrease in transport with depth (Storms et al., 2002; Cowell and Kinsela, 2018). More sophisticated methods for lower shoreface change may be introduced as data validation becomes available (e.g., Aagaard, 2011).

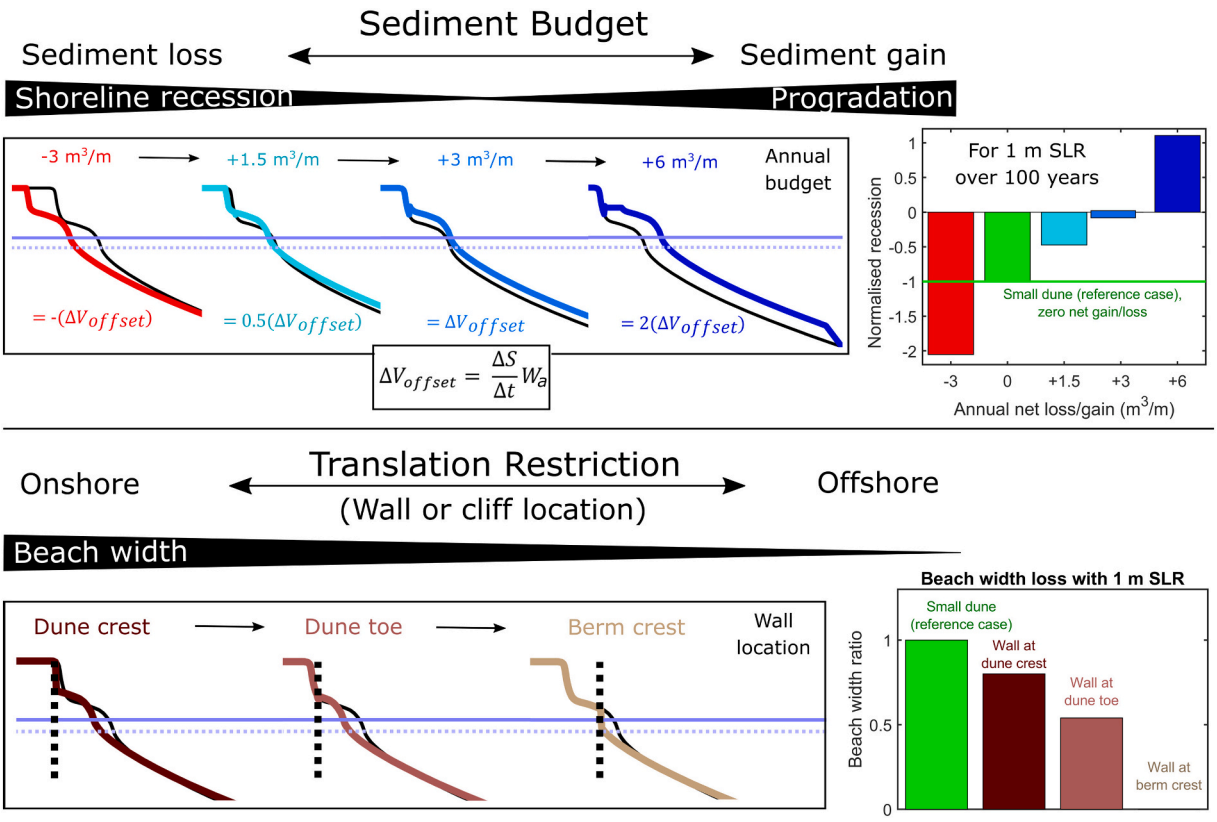

Fig. 18. (Top) Recession rates for a range of sediment loss/gain scenarios, relative to the reference case. (Bottom) Beach width loss for a range of wall/cliff positions, relative to the reference case. 'Reference Case' is profile #6 in Fig. 16.

6.3.2. Wave forcing and variations in wave climate

As a standalone method, ShoreTrans cannot be used to estimate instantaneous short-term shoreline variability or the impacts of changes in future wave climates, or the uncertainty around these impacts (Toimil et al., 2020). However, the tool has been designed with the intention that it may be added to existing hybrid modelling approaches (e.g., Toimil et al., 2017; Vitousek et al., 2017a; Antolínez et al., 2019), that incorporate wave and water level time series forcing, and can therefore address potential changes in wave climate into future shoreline prediction. Coupling the ShoreTrans profile translation methods with a cross-shore / longshore forcing model would also allow for more sophisticated statistical approaches (Le Cozannet et al., 2019) to be incorporated into assessing the impacts of potential future wave climate and SLR rise scenarios.

6.3.3. Translation rules

The most significant limitation of this first iteration of the ShoreTrans approach is that barrier response is pre-determined and fixed, with the intent that the user define the inputs and apply the model to investigate the impacts of various translation responses. For example, at Start Bay (Fig. 2, Figs. 14-15), the future barrier response is uncertain, and a pre-defined exploratory tool is required. However, several existing models automatically adapt the barrier response based on the shoreface-barrier configuration and the angle of the substrate (e.g., STM of Cowell et al., 2003, b; GEOMBEST of Stolper et al., 2005; Wolinsky and Murray, 2009). Due to this limitation, ShoreTrans is not currently suitable to longer simulations ($>>$ 100 years), and must be used with caution where the response will change over time (e.g., where initial dune encroachment switches to barrier rollover), and will require a degree a expertise from the user to assess likely response type.

The four ShoreTrans options for barrier response (Table 1, 'rollover' to 'encroachment') are elementary but are suitable for a first-pass assessment of translation distances under various scenarios. Future developments could allow for a variable amount of barrier height growth relative to SLR. Barrier retreat is currently assumed to be zero in the absence of long-term SLR and/or changes to total profile volume (e.g., due to longshore transport gradients). In reality, low barriers can rollover during high wave and temporary high water level events, such as during hurricanes (e.g., Lorenzo-Trueba and Ashton, 2014). An option to include a rate of non-SLR related barrier response could be included in a future iteration.

6.3.4. Cliff erosion, soft-rocks, fine sediments and mixed sediments

ShoreTrans is limited to dealing with unconsolidated sediments or non-erodible walls and substrates. This may be a reasonable assumption for hard-rock cliffs, such as those at Perranporth, where cliff-erosion rates are negligible over *O*(100 year) timescales. For soft-rock cliffs and semi-consolidated sediments (e.g., Walkden and Hall, 2011; Brooks and Spencer, 2014; Kinsela et al., 2017), rapid erosion rates can occur, providing a source of sediment that may partially offset recession (Wolinsky and Murray, 2009).

For soft-cliff erosion and lower shoreface transport, the disturbed sediment may contain a portion of fine-grained sediment that remains suspended in the water column and is carried away from the active profile, which is particularly important for barriers translating into buried lagoon deposits (Cowell et al., 1995; Cowell et al., 2003, b; Wolinsky and Murray, 2009). This was not a relevant process in the applications presented here but should be included in a future iteration. Similarly, mixed sediment classes and compound sand and gravel shorefaces could be included, though are beyond the present scope. For example, nourishments with a different grain size to the native sediment may change depth of closure or equilibrium profile shape.

6.3.5. Estuarine sediment flux

Coasts interrupted by inlets to estuaries can experience significant sediment fluxes between the shoreface and the estuary (e.g., Cowell

et al., 2003, b; Ranasinghe et al., 2013). A straightforward method of estimating the sediment budget demand of estuaries under SLR is to simply multiply the area of the flood tide delta by the change in sea level (e.g., Kinsela et al., 2017; Toimil et al., 2017). That approach could be incorporated into ShoreTrans by modifying the source/sink term (ΔV_{SS}, Eq. 7). More complex approaches (e.g., Ranasinghe et al., 2013; Bamunawala et al., 2020) would require ShoreTrans to be coupled with another model. Additionally, backbarrier infilling by fluvial and catchment processes is absent from the model at present, though that mode of barrier response is prevalent in some settings (Moore et al., 2010; Walters et al., 2014; Brenner et al., 2015)), and in that case, ShoreTrans is not suitable for application.

6.4. Implications for future investigations of shoreline change

A primary contribution of this work is to provide a simple means of predicting a translated surveyed (non-parameterised) 2D-profile that accounts for complexities and irregularities such as walls, rocks and varying barrier shapes. This can then be used to resolve issues over use of a particular translation formula (e.g., Standard Bruun-encroachment vs. Modified Bruun-rollover), and can further be used to test assumptions and the relative importance of various input factors (e.g., dune height and shape), as well as the dominant control on shoreline change (SLR effects, cross-shore variability or long-term trends). The tool is well-suited to a future investigation of how variation/uncertainty in inputs contribute to variation in predicted recession rates, both at the shoreline and the dune toe, and could be included in existing one-line reduced complexity modelling approaches (Toimil et al., 2017; Vitousek et al., 2017a; Antolínez et al., 2019; Le Cozannet et al., 2019).

Additionally, we seek to add clarity to the debate on whether beaches are in danger of becoming "extinct" under a given level of sea level rise (e.g., Vitousek et al., 2017c; Vousdoukas et al., 2020; Cooper et al., 2020). The issue here is not simply the application of the Bruun rule; our work suggests that Bruun is a good first-pass estimate (Figs. 12, 16, 17) provided trend rates of shoreline change, incorporating all aspects of sediment budget, are accounted for. This is consistent with other investigations (Dean and Houston, 2016, provide a summary). The key factor often omitted when predicting coastal evolution is onshore accommodation space, i.e., can the barrier translate onshore by eroding a dune or rolling back a barrier, or will this translation be cut-off by a seawall or hard-rock cliff? The key statistic here is *beach width*, not *shoreline recession*. Under the assumption that the active profile is able to translate much faster than sea level rise, narrow beaches backed by seawalls or cliffs are at imminent risk (e.g., Torcross, Fig. 16), wider beaches backed by cliffs or walls will begin to lose beach width under higher rates of sea level rise (e.g., mid to north Perranporth, Figs. 11-13; Manly, Australia; Cowell et al., 2006), while dune-backed beaches are unlikely to lose any beach width (south Perranporth, Fig. 10). For beaches backed by infrastructure, such as where houses are built within the active profile (e.g., Narrabeen, Australia; Beuzen et al., 2019), there is risk of losing beach width if the infrastructure is defended ("Hold the line" policy in the UK; Masselink et al., 2020), but the beach will survive if infrastructure is removed ("Managed retreat"), or alternatively if the beach is sufficiently nourished (e.g., Dean and Houston, 2016). Accordingly, the next report on the future of the world's beaches should focus on beach width, as well as shoreline recession, and the methods described here provide a means with which to address this question of vital public interest.

7. Conclusions

A simple shoreface translation and sediment budgeting tool (ShoreTrans) was introduced, capable of rapid, first-pass estimates of future coastal change in 2D for a wide range of profile types. This approach can incorporate dune erosion, barrier rollover, seawalls and rocky substrates, exchange with the lower shoreface, alongshore redistribution of dune erosion within embayments as well as other inputs and outputs to the sediment budget, e.g., longshore transport. The methods also incorporate probabilistic uncertainty and estimates of short-term shoreline variability. A novel aspect is the use of the full cross-shore profile, as opposed to a parameterisation, making it well suited to examining the impact of unusual features such as perched dunes and complex defended profiles.

The translation model was applied to two extensively studied macrotidal sites: Perranporth and Start Bay, in southwest UK. When compared to the standard Bruun rule approach, the translation model predicted reduced recession rates for dune-backed profiles, increased recession rates for sea-wall and cliff-backed profiles, as well as increased recession for lagoon-backed barriers, where rollover is predicted.

In contrast to most existing methods, ShoreTrans provides a prediction of how beach width will change due to sea level rise. In this regard, narrow beaches (<50 m) backed by sea-walls are most likely to become extinct given ~1-m of sea level rise, wider beaches backed by cliffs or walls will see moderate reductions (10–50% loss of beach width), while dune backed beaches and barriers that effectively rollback with sea level rise are unlikely to lose any beach width. The concept of reduced beach width is critical when addressing future impacts on global shorelines, and this simple tool offers coastal researchers a quick and easy means to make that assessment, in particular if combined with an existing reduced complexity model.

Declaration of Competing Interest

The authors declare that they have no known competing financial interests or personal relationships that could have appeared to influence the work reported in this paper.

Acknowledgements

This work was funded by a NERC Special Highlights Grant (NE/M004996/1; BLUE-coast project) and an EPSRC Overseas Travel Grant (EP/T004304/1; Coastal Modelling of Extreme Storms and Sea level Rise). Many thanks to Plymouth Coastal Observatory and the BlueCoast team for data collection. A sincere thank you to Sean Vitousek and an anonymous reviewer, who provided thorough and knowledgeable critiques, substantially reshaping and improving the manuscript. Data and Matlab code written for personal use are available on the University of Plymouth PEARL data repository. A public version of the ShoreTrans code is available at https://github.com/jakmccarroll/ShoreTrans.

References

Aagaard, Troels, 2011. Sediment transfer from beach to shoreface: The sediment budget of an accreting beach on the Danish North Sea Coast. Geomorphology 135, 143–157.
Anthony, E.J., Aagaard, T., 2020. The lower shoreface: morphodynamics and sediment connectivity with the upper shoreface and beach. Earth Sci. Rev. 103334.
Antolínez, J.A., Méndez, F.J., Anderson, D., Ruggiero, P., Kaminsky, G.M., 2019. Predicting climate-driven coastlines with a simple and efficient multiscale model. J. Geophys. Res. Earth Surf. 124 (6), 1596–1624.
Atkinson, A.L., Baldock, T.E., Birrien, F., Callaghan, D.P., Nielsen, P., Beuzen, T., Ranasinghe, R., 2018. Laboratory investigation of the Bruun rule and beach response to sea level rise. Coast. Eng. 136, 183–202.
Bamunawala, J., Dastgheib, A., Ranasinghe, R., van der Spek, A., Maskey, S., Murray, A. B., Sirisena, T.A.J.G., 2020. A holistic modeling approach to project the evolution of inlet-interrupted coastlines over the 21st century. Front. Mar. Sci. 7, 542.
Beuzen, T., Turner, I.L., Blenkinsopp, C.E., Atkinson, A., Flocard, F., Baldock, T.E., 2018. Physical model study of beach profile evolution by sea level rise in the presence of seawalls. Coast. Eng. 136, 172–182.
Beuzen, T., Harley, M.D., Splinter, K.D., Turner, I.L., 2019. Controls of variability in berm and dune storm erosion. J. Geophys. Res. Earth Surf. 124 (11), 2647–2665.
Brenner, O.T., Moore, L.J., Murray, A.B., 2015. The complex influences of back-barrier deposition, substrate slope and underlying stratigraphy in barrier island response to sea-level rise: Insights from the Virginia Barrier Islands, Mid-Atlantic Bight, USA. Geomorphology 246, 334–350.
Brooks, S.M., Spencer, T.S., 2014. Importance of decadal scale variability in shoreline response: examples from soft rock cliffs, East Anglian coast, UK. J. Coast. Conserv. 18, 581–593. https://doi.org/10.1007/s11852-013-0279-7.

Bruun, P., 1954. Coast Erosion and the Development of Beach Profiles, Vol. 44. US Beach Erosion Board.
Bruun, P., 1962. Sea level rise as a cause of shore erosion. J. Waterways Harbors Div. 88 (1), 117–132.
Bruun, P., 1988. The Bruun rule of erosion by sea level rise: a discussion on large-scale two-and three-dimensional usages. J. Coast. Res. 627–648.
Cooper, J.A.G., Pilkey, O.H., 2004. Sea level rise and shoreline retreat: time to abandon the Bruun rule. Glob. Planet. Chang. 43 (3–4), 157–171.
Callaghan, D, Nielsen, P, Short, A, Ranasinghe, R, 2008. Statistical simulation of wave climate and extreme beach erosion. Coast. Eng. 55, 375–390.
Cooper, A., Masselink, G., Coco, G., Short, A., Castelle, B., Rogers, K., Jackson, D., 2020. Sandy beaches can survive sea level rise.
Cowell, P.J., Kinsela, M.A., 2018. Shoreface controls on barrier evolution and shoreline change. In: Barrier Dynamics and Response to Changing Climate. Springer, Cham, pp. 243–275.
Cowell, P.J., Roy, P.S., Jones, R.A., 1992. Shoreface translation model: computer simulation of coastal-sand-body response to sea level rise. Math. Comput. Simul. 33 (5–6), 603–608.
Cowell, P.J., Roy, P.S., Jones, R.A., 1995. Simulation of large-scale coastal change using a morphological behaviour model. Mar. Geol. 126 (1–4), 45–61.
Cowell, Peter J., Stive, Marcel J.F., Roy, Peter S., Kaminsky, George M., Buijsman, Maarten C., Thom, Bruce G., Wright, L. Don, 2001. Shoreface sand supply to beaches. In: Coastal Engineering, 2000, pp. 2495–2508.
Cowell, P.J., Stive, M.J., Niedoroda, A.W., de Vriend, H.J., Swift, D.J., Kaminsky, G.M., Capobianco, M., 2003a. The coastal-tract (part 1): a conceptual approach to aggregated modeling of low-order coastal change. J. Coast. Res. 812–827.
Cowell, P.J., Stive, M.J., Niedoroda, A.W., Swift, D.J., de Vriend, H.J., Buijsman, M.C., Reed, C.W., 2003b. The coastal-tract (part 2): applications of aggregated modeling of lower-order coastal change. J. Coast. Res. 828–848.
Cowell, P.J., Thom, B.G., Jones, R.A., Everts, C.H., Simanovic, D., 2006. Management of uncertainty in predicting climate-change impacts on beaches. J. Coast. Res. 232–245.
Daley, M., Cowell, P.J., 2012. Long-term shoreface response to disequilibrium-stress: a conundrum for climate change 2. Stress (Wright 1995) 84, 85.
Davidson, M.A., Lewis, R.P., Turner, I.L., 2010. Forecasting seasonal to multi-year shoreline change. Coast. Eng. 57 (6), 620–629.
de Alegria-Arzaburu, A.R., Masselink, G., 2010. Storm response and beach rotation on a gravel beach, Slapton Sands, UK. Mar. Geol. 278 (1–4), 77–99.
Dean, R.G., 1977. Equilibrium Beach Profiles: US Atlantic and Gulf Coasts. Department of Civil Engineering and College of Marine Studies, University of Delaware.
Dean, R.G., Houston, J.R., 2016. Determining shoreline response to sea level rise. Coast. Eng. 114, 1–8.
Dean, R.G., Maurmeyer, E.M., 1983. Models for beach profile response. In: Handbook of Coastal Processes and Erosion. Edited by PD Komar.
Erikson, L.H., O'Neill, A., Barnard, P.L., Vitousek, S., Limber, P., 2017. Climate change-driven cliff and beach evolution at decadal to centennial time scales. Coast. Dyn. 2017, 125–136.
Fruergaard, M., Møller, I., Johannessen, P.N., Nielsen, L.H., Andersen, T.J., Nielsen, L., Pejrup, M., 2015. Stratigraphy, evolution, and controls of a Holocene transgressive–regressive barrier island under changing sea level: Danish North Sea coast. J. Sediment. Res. 85 (7), 820–844.
Fruergaard, M., Sander, L., Goslin, J., Andersen, T.J., 2021. Temporary late Holocene barrier-chain deterioration due to insufficient sediment availability, Wadden Sea, Denmark. Geology 49 (2), 162–167.
Hails, J.R., 1975. Submarine geology, sediment distribution and Quaternary history of Start Bay, Devon. J. Geol. Soc. 131 (1), 1–5.
Hallermeier, R.J., 1981. A profile zonation for seasonal sand beaches from wave climate. Coast. Eng. 4 (C), 253–277.
Harley, M.D., Turner, I.L., Short, A.D., Ranasinghe, R., 2011. A reevaluation of coastal embayment rotation: the dominance of cross-shore versus alongshore sediment transport processes, Collaroy-Narrabeen Beach, Southeast Australia. J. Geophys. Res. Earth Surf. 116 (F4).
Hoonhout, B.M., Vries, S.D., 2016. A process-based model for aeolian sediment transport and spatiotemporal varying sediment availability. J. Geophys. Res. Earth Surf. 121 (8), 1555–1575.
Kinsela, M.A., Daley, M.J., Cowell, P.J., 2016. Origins of Holocene coastal strandplains in Southeast Australia: shoreface sand supply driven by disequilibrium morphology. Mar. Geol. 374, 14–30.
Kinsela, M.A., Morris, B.D., Linklater, M., Hanslow, D.J., 2017. Second-pass assessment of potential exposure to shoreline change in New South Wales, Australia, using a sediment compartments framework. J. Mar. Sci. Eng. 5 (4), 61.
Kinsela, M.A., Hanslow, D.J., Carvalho, R.C., Linklater, M., Ingleton, T.C., Morris, B.D., Woodroffe, C.D., 2020. Mapping the shoreface of coastal sediment compartments to improve shoreline change forecasts in New South Wales, Australia. Estuar. Coasts 1–27.
Kriebel, D.L., Dean, R.G., 1993. Convolution method for time-dependent beach-profile response. J. Waterw. Port Coast. Ocean Eng. 119 (2), 204–226.
Le Cozannet, G., Oliveros, C., Castelle, B., Garcin, M., Idier, D., Pedreros, R., Rohmer, J., 2016. Uncertainties in sandy shorelines evolution under the Bruun rule assumption. Front. Mar. Sci. 3, 49.
Larson, M, Erikson, L, Hanson, H, 2004. An analytical model to predict dune erosion due to wave impact. Coast. Eng. 51, 675–696.
Le Cozannet, G., Bulteau, T., Castelle, B., Ranasinghe, R., Wöppelmann, G., Rohmer, J., Salas-y-Mélia, D., 2019. Quantifying uncertainties of sandy shoreline change projections as sea level rises. Sci. Rep. 9 (1), 1–11.
Lorenzo-Trueba, J., Ashton, A.D., 2014. Rollover, drowning, and discontinuous retreat: distinct modes of barrier response to sea-level rise arising from a simple morphodynamic model. J. Geophys. Res. Earth Surf. 119 (4), 779–801.
Loureiro, C., Ferreira, Ó., Cooper, J.A.G., 2012. Extreme erosion on high-energy embayed beaches: influence of megarips and storm grouping. Geomorphology 139, 155–171.
Luijendijk, A., Hagenaars, G., Ranasinghe, R., Baart, F., Donchyts, G., Aarninkhof, S., 2018. The state of the world's beaches. Sci. Rep. 8 (1), 1–11.
Luijendijk, A.P., de Schipper, M.A., Ranasinghe, R., 2019. Morphodynamic acceleration techniques for multi-timescale predictions of complex sandy interventions. J. Mar. Sci. Eng. 7 (3), 78.
Masetti, R., Fagherazzi, S., Montanari, A., 2008. Application of a barrier island translation model to the millennial-scale evolution of Sand Key, Florida. Cont. Shelf Res. 28 (9), 1116–1126.
Masselink, G., Scott, T., Poate, T., Russell, P., Davidson, M., Conley, D., 2016. The extreme 2013/2014 winter storms: hydrodynamic forcing and coastal response along the southwest coast of England. Earth Surf. Process. Landf. 41 (3), 378–391.
Masselink, G., Russell, P., Rennie, A., Brooks, S., Spencer, T., 2020. Impacts of climate change on coastal geomorphology and coastal erosion relevant to the coastal and marine environment around the UK. MCCIP Sci. Rev. 2020, 158–189.
McCarroll, R.J., Brander, R.W., Turner, I.L., Van Leeuwen, B., 2016. Shoreface storm morphodynamics and mega-rip evolution at an embayed beach: Bondi Beach, NSW, Australia. Cont. Shelf Res. 116, 74–88.
McCarroll, R.J., Masselink, G., Valiente, N.G., Scott, T., King, E.V., Conley, D., 2018. Wave and tidal controls on embayment circulation and headland bypassing for an exposed, macrotidal site. J. Mar. Sci. Eng. 6 (3), 94.
McCarroll, R.J., Masselink, G., Wiggins, M., Scott, T., Billson, O., Conley, D.C., Valiente, N.G., 2019a. High-efficiency gravel longshore sediment transport and headland bypassing over an extreme wave event. Earth Surf. Process. Landf. 44 (13), 2720–2727.
McCarroll, R.J., Masselink, G., Wiggins, M., Scott, T., Billson, O., Conley, D., 2019b. Gravel Beach Cross- and Alongshore Response to an Extreme Event: Beach Length and Headland Proximity Controls.
McCarroll, R.J., Masselink, G., Valiente, N.G., Wiggins, M., Scott, T., Conley, D.C., King, E.V., 2020. Impact of a headland-associated sandbank on shoreline dynamics. Geomorphology 355, 107065.
Mentaschi, L., Vousdoukas, M.I., Pekel, J.F., Voukouvalas, E., Feyen, L., 2018. Global long-term observations of coastal erosion and accretion. Sci. Rep. 8 (1), 1–11.
Montaño, J., Coco, G., Antolínez, J.A., Beuzen, T., Bryan, K.R., Cagigal, L., Idier, D., 2020. Blind testing of shoreline evolution models. Sci. Rep. 10 (1), 1–10.
Moore, L.J., List, J.H., Williams, S.J., Stolper, D., 2010. Complexities in barrier island response to sea level rise: Insights from numerical model experiments, North Carolina Outer Banks. J. Geophys. Res. Earth Surf. 115 (F3).
Nielsen, A.F., Lord, D.B., Poulos, H.G., 1992. Dune stability considerations for building foundations. Civil Eng. Trans. Inst. Eng. Aust CE34, 167–174, 1992.
Orford, J.D., Carter, R.W.G., Jennings, S.C., Hinton, A.C., 1995. Processes and timescales by which a coastal gravel-dominated barrier responds geomorphologically to sea-level rise: Story head barrier, Nova Scotia. Earth Surf. Process. Landf. 20 (1), 21–37.
Plant, N.G., Stockdon, H.F., 2012. Probabilistic prediction of barrier-island response to hurricanes. J. Geophys. Res. Earth Surf. 117 (F3).
Poate, T., Masselink, G., Russell, P., Austin, M., 2014. Morphodynamic variability of high-energy macrotidal beaches, Cornwall, UK. Mar. Geol. 350, 97–111.
Ranasinghe, R., 2020. On the need for a new generation of coastal change models for the 21st century. Sci. Rep. 10 (1), 1–6.
Ranasinghe, R., Callaghan, D., Stive, M.J., 2012. Estimating coastal recession due to sea level rise: beyond the Bruun rule. Clim. Chang. 110 (3–4), 561–574.
Ranasinghe, R., Duong, T.M., Uhlenbrook, S., Roelvink, D., Stive, M., 2013. Climate-change impact assessment for inlet-interrupted coastlines. Nat. Clim. Chang. 3, 83–87.
Robinet, A., Idier, D., Castelle, B., Marieu, V., 2018. A reduced-complexity shoreline change model combining longshore and cross-shore processes: the LX-Shore model. Environ. Model. Softw. 109, 1–16.
Robinet, A., Castelle, B., Idier, D., Harley, M.D., Splinter, K.D., 2020. Controls of local geology and cross-shore/longshore processes on embayed beach shoreline variability. Mar. Geol. 106118.
Roelvink, D., Costas, S., 2019. Coupling nearshore and aeolian processes: XBeach and Duna process-based models. Environ. Model. Softw. 115, 98–112.
Rosati, J.D., 2005. Concepts in sediment budgets. J. Coast. Res. 21, 307–322 (2 (212)).
Rosati, J.D., Dean, R.G., Walton, T.L., 2013. The modified Bruun rule extended for landward transport. Mar. Geol. 340, 71–81.
Roy, P.S., Cowell, P.J., Ferland, M.A., Thom, B.G., 1994. Wave dominated coasts. In: RWG, Carter, Woodroffe, C.D. (Eds.), Coastal Evolution: Late Quaternary Shoreline Morphodynamics. Cambridge University Press, Cambridge, pp. 121–186.
Sallenger Jr., A.H., 2000. Storm impact scale for barrier islands. J. Coast. Res. 890–895.
Scott, T., Masselink, G., McCarroll, R.J., Castelle, B., Dodet, G., Saulter, A., Scaife, A., Dunstone, N.J., 2021. Atmospheric controls and long range predictability of directional waves in the United Kingdom & Ireland. Earth's Future. https://doi.org/10.1002/essoar.10503076.1. In press.
Scott, T., Masselink, G., O'Hare, T., Saulter, A., Poate, T., Russell, P., Conley, D., 2016. The extreme 2013/2014 winter storms: beach recovery along the southwest coast of England. Mar. Geol. 382, 224–241.
Stive, M.J., 2004. How important is global warming for coastal erosion? Clim. Chang. 64 (1–2), 27.
Stive, M.J., De Vriend, H.J., 1995. Modelling shoreface profile evolution. Mar. Geol. 126 (1–4), 235–248.

Stokes, C., Davidson, M., Russell, P., 2015. Observation and prediction of three-dimensional morphology at a high-energy macrotidal beach. Geomorphology 243, 1–13.
Stolper, D., List, J.H., Thieler, E.R., 2005. Simulating the evolution of coastal morphology and stratigraphy with a new morphological-behaviour model (GEOMBEST). Mar. Geol. 218 (1–4), 17–36.
Storms, J.E., Weltje, G.J., Van Dijke, J.J., Geel, C.R., Kroonenberg, S.B., 2002. Process-response modeling of wave-dominated coastal systems: simulating evolution and stratigraphy on geological timescales. J. Sediment. Res. 72 (2), 226–239.
Thom, B.G., Bowman, G.M., Roy, P.S., 1981. Late Quaternary evolution of coastal sand barriers, Port Stephens-Myall Lakes area, Central New South Wales, Australia. Quat. Res. 15 (3), 345–364.
Toimil, A., Losada, I.J., Camus, P., Diaz-Simal, P., 2017. Managing coastal erosion under climate change at the regional scale. Coast. Eng. 128, 106–122.
Toimil, A., Camus, P., Losada, I.J., Le Cozannet, G., Nicholls, R.J., Idier, D., Maspataud, A., 2020. Climate change-driven coastal erosion modelling in temperate sandy beaches: methods and uncertainty treatment. Earth Sci. Rev. 202, 103110.
Turner, I.L., Harley, M.D., Short, A.D., Simmons, J.A., Bracs, M.A., Phillips, M.S., Splinter, K.D., 2016. A multi-decade dataset of monthly beach profile surveys and inshore wave forcing at Narrabeen, Australia. Sci. Data 3 (1), 1–13.
USACE, 2002. Shore Protection Manual. Coastal Engineering Research Center, Government Printing Office, Washington DC.
Valiente, N.G., Masselink, G., Scott, T., Conley, D., McCarroll, R.J., 2019a. Role of waves and tides on depth of closure and potential for headland bypassing. Mar. Geol. 407, 60–75.
Valiente, N.G., McCarroll, R.J., Masselink, G., Scott, T., Wiggins, M., 2019b. Multi-annual embayment sediment dynamics involving headland bypassing and sediment exchange across the depth of closure. Geomorphology 343, 48–64.
Valiente, N.G., Masselink, G., McCarroll, R.J., Scott, T., Conley, D., King, E., 2020. Nearshore sediment pathways and potential sediment budgets in embayed settings over a multi-annual timescale. Mar. Geol. 106270.
Vinent, O.D., Moore, L.J., 2015. Barrier island bistability induced by biophysical interactions. Nat. Clim. Chang. 5 (2), 158–162.
Vitousek, S., Barnard, P.L., Limber, P., Erikson, L., Cole, B., 2017a. A model integrating longshore and cross-shore processes for predicting long-term shoreline response to climate change. J. Geophys. Res. Earth Surf. 122 (4), 782–806.
Vitousek, S., Barnard, P.L., Fletcher, C.H., Frazer, N., Erikson, L., Storlazzi, C.D., 2017b. Doubling of coastal flooding frequency within decades due to sea level rise. Sci. Rep. 7 (1), 1–9.
Vitousek, S., Barnard, P.L., Limber, P., 2017c. Can beaches survive climate change? J. Geophys. Res. Earth Surf. 122 (4), 1060–1067.
Vos, K., Splinter, K.D., Harley, M.D., Simmons, J.A., Turner, I.L., 2019. CoastSat: a Google Earth Engine-enabled Python toolkit to extract shorelines from publicly available satellite imagery. Environ. Model. Softw. 122, 104528.
Vousdoukas, M.I., Ranasinghe, R., Mentaschi, L., Plomaritis, T.A., Athanasiou, P., Luijendijk, A., Feyen, L., 2020. Sandy coastlines under threat of erosion. Nat. Clim. Chang. 10 (3), 260–263.
Wainwright, D.J., Ranasinghe, R., Callaghan, D.P., Woodroffe, C.D., Jongejan, R., Dougherty, A.J., Cowell, P.J., 2015. Moving from deterministic towards probabilistic coastal hazard and risk assessment: Development of a modelling framework and application to Narrabeen Beach, New South Wales, Australia. Coast. Eng. 96, 92–99.
Walkden, M.J., Hall, J.W., 2011. A mesoscale predictive model of the evolution and management of a soft-rock coast. J. Coast. Res. 27 (3), 529–543.
Walters, D., Moore, L.J., Duran Vinent, O., Fagherazzi, S., Mariotti, G., 2014. Interactions between barrier islands and backbarrier marshes affect island system response to sea level rise: Insights from a coupled model. J. Geophys. Res. Earth Surf. 119 (9), 2013–2031.
Wiggins, M., Scott, T., Masselink, G., Russell, P., Castelle, B., Dodet, G., 2017. The role of multi-decadal climate variability in controlling coastal dynamics: re-interpretation of the 'lost village of Hallsands'. In: Coastal Dynamics, pp. 96–107.
Wiggins, M., Scott, T., Masselink, G., Russell, P., McCarroll, R.J., 2019. Coastal embayment rotation: response to extreme events and climate control, using full embayment surveys. Geomorphology 327, 385–403.
Wolinsky, M.A., 2009. A unifying framework for shoreline migration: 1. Multiscale shoreline evolution on sedimentary coasts. J. Geophys. Res. Earth Surf. 114 (F1).
Wolinsky, M.A., Murray, A.B., 2009. A unifying framework for shoreline migration: 2. Application to wave-dominated coasts. J. Geophys. Res. Earth Surf. 114 (F1).
Zhang, K., Douglas, B.C., Leatherman, S.P., 2004. Global warming and coastal erosion. Clim. Chang. 64 (1–2), 41.